



Seascape-level variation in turbulence- and wave-generated hydrodynamic signals experienced by plankton



Heidi L. Fuchs^{a,*}, Gregory P. Gerbi^b

^a Department of Marine and Coastal Sciences, Rutgers University, New Brunswick, NJ 08901, United States

^b Skidmore College, Saratoga Springs, NY 12866, United States

ARTICLE INFO

Article history:

Received 16 July 2015

Received in revised form 22 December 2015

Accepted 22 December 2015

Available online 29 December 2015

ABSTRACT

Plankton exhibit diverse and dramatic responses to fluid motions, and these behaviors are likely critical for survival and fitness. Fluid motions can be generated by organisms or by physical processes, including turbulence and surface gravity waves. Physical processes vary geographically in their intensity and generate hydrodynamic signals experienced by plankton as fluid forces on their sensory receptors. In this synthesis, we review how turbulence and waves vary in space, the scales and statistics of their motions, and the forces exerted on plankton. We then quantify the hydrodynamic signals produced by turbulence and waves in four seascape types – surf zones, inlets and estuaries, the continental shelf, and the open ocean – using published dissipation rates, wind and wave data from buoys, and observations from two coastal sites in Massachusetts, USA. We relate these geographic patterns in signals to the observed behaviors of example species and to the forces sensed by typical plankters with different receptor types. Turbulence-generated shears are largest in the surf zone, inlets and estuaries, while wave-generated accelerations are larger offshore; as a result, each seascape exhibits some range of combined shears and accelerations that is distinct. These signals generate forces on plankton that vary among habitats and with plankton size and swimming speed. Spatial patterns in fluid forces create a potential mechanism for dispersing larvae to distinguish habitats by their hydrodynamic signatures. However, turbulence can be strong in all seascapes and may cause widespread interference in signaling among predators and prey. Plankton with a single receptor type could identify nearshore habitats, while those with multiple receptor types potentially could distinguish inshore vs. offshore seascapes or decode signals produced by physical processes and by other organisms.

© 2015 Elsevier Ltd. All rights reserved.

1. Introduction

Microscopic plankton exhibit diverse reactions to fluid motions, and flow-induced behaviors may be critical for the survival and success of drifting organisms that use physical signals to find prey, to avoid predators, or to exploit currents for transport. In the life-or-death interactions among predators and prey, physical signals are considered the most effective means of communication. Predator or prey movements cannot be seen by zooplankton with simple visual systems, and chemical signals are transmitted by diffusion too slowly to warn of approaching plankters or particles; in contrast, flow sensing is feasible for organisms of at least a few micrometers in length (Martens et al., 2015), and fluid motions can be transmitted and perceived rapidly (reviewed by Kjørboe, 2011; Kjørboe, 2013). Water motions cause some zooplankton to jump away or attack, enabling them to avoid predators or to cap-

ture prey (Feigenbaum and Reeve, 1977; Fields and Yen, 1997; Kjørboe, 2013). Fluid motions also induce bioluminescent flashes in some phytoplankton that could startle their zooplankton predators or alert larger predators to their presence (e.g., Esaias and Curl, 1972; Latz et al., 2004; Haddock et al., 2010). However, plankton react to fluid motions regardless of whether they are generated by organisms or by physical processes such as turbulence and surface gravity waves. At sea, predator–prey communications may often be disrupted by interference from background turbulence (e.g., Singarajah, 1975; Lang, 1980; Costello et al., 1990; Visser, 2001).

Although environmental fluid motions act as noise in the context of predator–prey signaling, they may also act as sensory signals enabling migration into or away from particular environmental conditions. Some plankton migrate downward in the presence of strong wind-induced turbulence, avoiding high contact rates with predators near the surface and limiting flow-induced damage or disruption of swimming orientation (e.g., Barile et al., 1994; Incze et al., 2001; Rakow and Graham, 2006).

* Corresponding author.

E-mail address: hfuchs@marine.rutgers.edu (H.L. Fuchs).

Invertebrate larvae exhibit flow-induced changes in vertical swimming behaviors (Welch and Forward, 2001; Kingsford et al., 2002; Fuchs et al., 2013, 2015b) that could enhance larval supply to settlement sites in energetic coastal habitats (Fuchs et al., 2007; Fuchs and Reidenbach, 2013; Fujimura et al., 2014). Recent work has also begun to highlight how larvae are affected by wave motions, both within and beyond the surf zone (Reidenbach et al., 2009; Gaylord et al., 2013; Koehl et al., 2013; Fuchs et al., 2015b). Turbulence and waves have the potential to act as both sensory signals and noise but vary in their intensity among ocean regions, and there has been no systematic study of how this geographic variation is experienced by plankton.

Plankton research is sometimes presented in the context of geographic variation in turbulence using generalizations that lag advances in physical oceanography. Turbulence is typically quantified by the rate ε at which turbulent kinetic energy is dissipated to heat, a useful metric for summarizing the nature of small-scale fluid motions. The notion persists that ε is 100–1000 times lower in mixed layers in the open ocean than in coastal waters (Kiørboe and Saiz, 1995; Fuchs et al., 2004; Geyer et al., 2008). However, this concept of weaker turbulence offshore stems from a few classic observations that omitted measurements near the seabed or surface or in wavy conditions. This data gap is being addressed as technology evolves. Theory also has evolved, and our understanding of turbulence scaling near the surface has shifted from a classic boundary layer model, dependent only on the wind stress and depth (MacKenzie and Leggett, 1993), to models that account for surface wave characteristics (Agrawal et al., 1992; Craig and Banner, 1994; Terray et al., 1996). These developments in physical oceanography have been slow to permeate ecological understanding, and physical measurements are rarely presented in a form that is directly relevant to plankton.

The intensities of turbulence and waves are typically assessed using quantities that plankton experience only indirectly: turbulence is characterized by the dissipation rate, and waves are characterized by their amplitude and frequency. Plankton experience small-scale signals of these processes more directly in the form of instantaneous spatial and temporal velocity gradients (shears and accelerations) (Fig. 1). These hydrodynamic signals are detectable when they exert sufficient forces to mechanically displace a plankton's external or internal sensory receptors relative to the body (Budelmann, 1989). External mechanoreceptors detect fluid deformation and include setae of copepods, cilia of invertebrate larvae, and membrane-bound receptors in protists (e.g., Naitoh and Eckert, 1969; Mackie et al., 1976; Yen et al., 1992). Internal gravity receptors or accelerometers detect changes in body orientation or speed and include Müller vesicles in ciliates and statocysts in invertebrates (reviewed by Budelmann, 1988). Some common taxa lack internal accelerometers but can sense vibrations of external sensors (Feigenbaum and Reeve, 1977; Heuch and Karlsen, 1997). The hydrodynamic signals used, threshold values, and reactions are as diverse as species' sensing mechanisms, behavioral functions, and habitat requirements; for example, escape jumps have been observed at signal thresholds with corresponding dissipation rates spanning over three orders of magnitude (e.g., Fields and Yen, 1997; Kiørboe et al., 1999; Jakobsen, 2001, 2002; Burdick et al., 2007). We will review this behavioral variation in a separate publication. Here we focus on synthesizing statistical patterns in physical signals and forces that plankton experience due to geographic variation in the intensity of turbulence and waves.

Four major regions are proposed as potentially distinct hydrodynamic seascapes: the surf zone, inlets and estuaries, the continental shelf, and the open ocean. Finer habitat divisions are possible but may be useful only if there are hydrodynamic distinctions among major regions. Section 2 reviews the physical

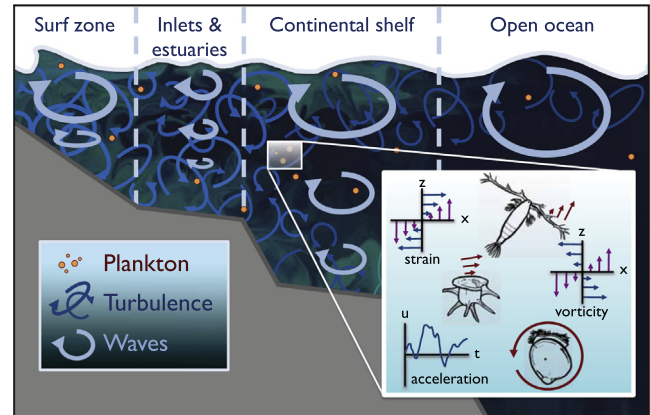


Fig. 1. Cartoon summarizing this study. Turbulence and wave motions vary in intensity among seascapes and produce velocity gradients experienced by plankton as hydrodynamic signals (inset). Not to scale.

processes that generate spatial variation in turbulence and waves (Section 2.1), the scales and statistics of hydrodynamic signals generated (Sections 2.2 and 2.3), and the associated hydrodynamic forces on plankton (Section 2.4), including calculations needed for quantifying hydrodynamic signals. Readers familiar with these topics may skip to Section 3, which describes the methods we used to compile observations of turbulence and waves, to analyze how turbulence- and wave-generated signals covary in space, and to express these spatially varying hydrodynamic signals as forces on planktonic organisms. The results (Section 4) quantify the spatial patterns in turbulence- and wave-generated signals and induced forces on representative plankters. The discussion (Section 5) presents these patterns as a conceptual framework for understanding how turbulence and waves affect hydrodynamic seascapes and plankton sensory ecology.

2. Environmental fluid motions

2.1. Spatial variations in turbulence and waves

Turbulence and waves may be distinguishing features of seascapes because they are generated by morphology and physical forcing with different spatial and temporal patterns. Most turbulence is generated in boundary layers, in shear layers, and by internal waves, and its intensity varies with tidal currents, winds, and stratification over hours to days. In the bottom boundary layer (BBL), turbulence can be caused by shear instability associated with tidal, wave-driven, or wind-driven currents (e.g., Sanford and Lien, 1999; Trowbridge et al., 1999; Rosman et al., 2008). In the surface boundary layer (SBL), turbulence can be caused by wind-driven shear instability or by whitecapping surface waves (Agrawal et al., 1992; Anis and Moum, 1995; Terray et al., 1996). In the surf zone, turbulence is generated by depth-limited wave breaking (George et al., 1994; Trowbridge and Elgar, 2001). Turbulence influences more of the water column in shallower water where tidal currents are stronger and the surface and bottom boundary layers can overlap.

Surface waves can be caused by local winds (wind sea) or propagate from remote areas (swell) and vary over hours to days. Swell tends to have longer periods, longer wavelengths, and larger orbital velocities than wind sea (Pierson and Moskowitz, 1964; Hasselmann et al., 1973), but whitecapping is more associated with wind sea than swell (Gerbi et al., 2009). In sheltered embayments and estuaries, the waves tend to be dominated by the local wind seas and are fetch-limited (Roberts et al., 2000; Jackson et al., 2002), although wind waves can be larger in channels and bays where the fetch is large (e.g., Stevens and Lacy, 2012). In coastal

regions exposed to the open ocean, either wind sea or swell can be the source of the dominant waves (Gargett et al., 2004; Styles and Glenn, 2005). Wave motions attenuate with depth, weakening to < 5% of their surface magnitudes within a depth of one half the wavelength, but their influence can reach the bottom boundary layer in coastal regions (Trowbridge and Madsen, 1984; Grant and Madsen, 1986; Koehl et al., 2013). Generally, waves are smaller in enclosed, shallow waters with a small fetch and larger and more energetic in open, deep waters where the fetch is unlimited.

Waves also can be a source of turbulent kinetic energy in the surface boundary layer through wind-driven whitecapping. Below depths of several wave heights, the dissipation rate follows the classic scaling for flow past a rigid boundary and can be estimated as

$$\varepsilon_r = \frac{u_*^3}{\kappa|z|} \quad (1)$$

where $u_* = (\tau/\rho_f)^{0.5}$ is shear velocity defined by the wind stress τ and the fluid density ρ_f , $\kappa = 0.4$ is von Karman's constant, and $|z|$ is distance to the boundary. Near the surface, however, wind-driven whitecapping injects energy into the boundary layer and raises the dissipation rate to approximately

$$\varepsilon_w = 0.3 \frac{c_e u_*^2 H_w}{z^2} \quad (2)$$

where c_e is the relative velocity at which energy is transferred from wind to waves (Gemrich et al., 1994; Terray et al., 1996; Hwang, 2009) and H_w is the significant height of the wind waves. This Eq. (2) typically gives larger values of dissipation rate than Eq. (1) within several wave heights of the surface.

2.2. Scales of motion

Turbulence and waves generate motions independently (e.g., Trowbridge, 1998) and on different scales, so they have different effects on hydrodynamic signals. Small-scale turbulence has dynamics related to the dissipation rate ε and the fluid's kinematic viscosity ν (Tennekes and Lumley, 1972; Jumars et al., 2009). The smallest eddies produce velocity gradients on spatial scales at and larger than the Kolmogorov scale η_k at which energy is dissipated, defined as

$$\eta_k = \left(\frac{\nu^3}{\varepsilon}\right)^{0.25} \quad (3)$$

with time scales τ_k and velocity scales v_k

$$\tau_k = \left(\frac{\nu}{\varepsilon}\right)^{0.5} \quad (4)$$

$$v_k = (\nu\varepsilon)^{0.25} \quad (5)$$

Kolmogorov scales are typically in the ranges $\eta_k \approx 10^{-4}$ – 10^{-2} m, $\tau_k \approx 0.01$ – 10 s, and $v_k \approx 10^{-4}$ – 10^{-2} m s⁻¹. These Kolmogorov-scale eddies produce shears and accelerations of order

$$\text{shear} \approx \frac{v_k}{\eta_k} \approx \left(\frac{\varepsilon}{\nu}\right)^{0.5} \quad (6)$$

$$\text{acceleration} \approx \frac{v_k}{\tau_k} \approx \left(\frac{\varepsilon^3}{\nu}\right)^{0.25} \quad (7)$$

respectively, where shears include deformational (e.g., strain rate) and rotational (vorticity) motions (Table 1). The highest shears tend to occur on length scales near η_k (Tennekes and Lumley, 1972). In turbulence, plankters will be able to sense any shears exceeding their detection limits over length scales at least as large as the sensing organs. Stronger turbulence produces both smaller eddies (Eq. (3)) and higher velocity gradients (Eq. (6), (7)) and is more detectable to plankters with a wider range of sizes and sensory mechanisms.

Compared to Kolmogorov-scale turbulence, wave motions vary on similar time scales but larger spatial and velocity scales. Velocity gradients are generated by orbital motions with wavelengths λ , wave amplitudes a , wave periods $T = 2\pi/\omega$, where ω is radian wave frequency, and orbital velocities \tilde{u}_{\max} , where $\tilde{u}_{\max} \approx 2\pi a/T$ at the surface. The two length scales describe how much energy is in the wave field (a) and the length scale on which that energy varies (λ). Wave motions typically have scales of $\lambda \approx 1$ – 100 s of m, $T \approx 1$ – 10 s, and $\tilde{u}_{\max} \approx 0.1$ – 1 m s⁻¹ or more (Mei, 1989; Traykovski, 2007). Outside the surf zone, wave motions are approximately linear (Phillips, 1966) and produce shears and accelerations of order

$$\text{shear} \approx a \left(\frac{2\pi}{\lambda}\right) \left(\frac{2\pi}{T}\right) \approx \frac{2\pi\tilde{u}_{\max}}{\lambda} \quad (8)$$

$$\text{acceleration} \approx a \left(\frac{2\pi}{T}\right)^2 \approx \frac{2\pi\tilde{u}_{\max}}{T} \quad (9)$$

respectively. For a given wave amplitude, shorter-period waves with smaller wavelengths produce larger shears and accelerations. In waves, shears act over wavelengths λ that are always larger than plankton, and detectability will be limited only by shear magnitude.

Because turbulence and waves have different scales of motion, they can produce velocity gradients, particularly accelerations, with disparate magnitudes. These magnitudes can be compared using Eqs. (6)–(9) to approximate when the velocity gradients produced by turbulence will exceed those produced by waves. If we set the quantities in Eqs. (6) and (7) greater than those in Eqs. (8) and (9) and rearrange, turbulence can produce larger velocity gradients than waves when

$$\text{shear} : \varepsilon > \frac{4\nu\pi^2\tilde{u}_{\max}^2}{\lambda^2} \quad (10)$$

$$\text{acceleration} : \varepsilon > \left(\frac{16\nu\pi^4\tilde{u}_{\max}^4}{T^4}\right)^{\frac{1}{3}} \quad (11)$$

Table 1

Representative 2-dimensional expressions for variances of shears and accelerations generated by isotropic turbulence (denoted by primes) and linear wave motions (denoted by tildes) (Taylor, 1935; Phillips, 1966; Voth et al., 2002). Symbols: Δ_{uz} – longitudinal deformation rate; Δ_{uz} – shear deformation rate; γ – strain rate; ξ – vorticity; α – acceleration; σ^2 – variance; ε – dissipation rate; ν – kinematic viscosity; a_0 – constant (≈ 5); k – wavenumber ($= 2\pi/\lambda$ where λ is wavelength); ω – wave frequency; S – sea-surface displacement spectrum; F and F' – vertical structure functions ($F = \cosh(k(z+h))/\sinh(kh)$, and $F' = \sinh(k(z+h))/\sinh(kh)$); z – vertical distance from mean sea surface; and h – water depth.

Signal		Turbulence	Waves
Shear deformation rate	$\Delta_{uz} = \frac{\partial u}{\partial z}$ or $\frac{\partial w}{\partial x}$	$\sigma_{\Delta_{uz}}^2 \approx \frac{\varepsilon}{7.5\nu}$	$\sigma_{\tilde{\Delta}_{uz}}^2 = \int_0^\infty d\omega k^2 \omega^2 S F^2(kz)$
Longitudinal deformation rate	$\Delta_{ux} = \frac{\partial u}{\partial x}$ or $\frac{\partial w}{\partial z}$	$\sigma_{\Delta_{ux}}^2 \approx \frac{\varepsilon}{15\nu}$	$\sigma_{\tilde{\Delta}_{ux}}^2 = \int_0^\infty d\omega k^2 \omega^2 S F^2(kz)$
Strain rate	$\gamma = \frac{1}{2} \left(\frac{\partial u}{\partial z} + \frac{\partial w}{\partial x} \right)$	$\sigma_{\gamma'}^2 \approx \frac{\varepsilon}{20\nu}$	$\sigma_{\tilde{\gamma}}^2 = \int_0^\infty d\omega k^2 \omega^2 S F^2(kz)$
Vorticity	$\xi = \frac{\partial w}{\partial x} - \frac{\partial u}{\partial z}$	$\sigma_{\xi'}^2 \approx \frac{\varepsilon}{3\nu}$	$\tilde{\xi} = 0$
Acceleration (horizontal)	$\alpha_u = \frac{\partial u}{\partial t}$	$\sigma_{\alpha'_u}^2 \approx a_0 \frac{\varepsilon^{1.5}}{\nu^{0.5}}$	$\sigma_{\tilde{\alpha}_u}^2 = \int_0^\infty d\omega \omega^4 S F^2(kz)$
Acceleration (vertical)	$\alpha_w = \frac{\partial w}{\partial t}$	$\sigma_{\alpha'_w}^2 \approx a_0 \frac{\varepsilon^{1.5}}{\nu^{0.5}}$	$\sigma_{\tilde{\alpha}_w}^2 = \int_0^\infty d\omega \omega^4 S F^2(kz)$

respectively. Assuming that wave motions have the typical scales given above, turbulence should dominate the production of shears at a broad range of dissipation rates ($\epsilon > 10^{-9}$ – 10^{-7} m² s⁻³; Eq. 10), whereas turbulence may dominate the production of accelerations only at the highest dissipation rates ($\epsilon > 10^{-4}$ – 0.1 m² s⁻³; Eq. 11).

2.3. Hydrodynamic signal statistics

The independent motions of turbulence and waves combine to produce the net fluid motions experienced by plankton. The relative contributions of turbulence and waves to small-scale motions can be quantified by decomposing the instantaneous flow velocity; for example u in the along-stream direction x becomes

$$u = U + u' + \tilde{u} \quad (12)$$

where U is velocity averaged over time and space, u' is the instantaneous velocity fluctuation due to turbulence, and \tilde{u} is the instantaneous velocity fluctuation due to wave oscillations. Similar decompositions apply to v and w in the cross-stream y and vertical z directions. Primes and tildes will be used throughout to denote turbulence and wave quantities, respectively. Taking space- or time-derivatives of Eq. (12) gives the instantaneous shears or accelerations due to turbulence and waves; for example,

$$\frac{\partial u}{\partial z} = 0 + \frac{\partial u'}{\partial z} + \frac{\partial \tilde{u}}{\partial z} \quad (13)$$

$$\frac{\partial u}{\partial t} = 0 + \frac{\partial u'}{\partial t} + \frac{\partial \tilde{u}}{\partial t} \quad (14)$$

where $\partial u/\partial z$ is shear deformation rate, abbreviated hereafter as Δ_{uz} , and $\partial u/\partial t$ is unidirectional acceleration, abbreviated hereafter as α_u (see Table 1 for velocity gradient definitions). These gradients are of the same order as other components of shear and acceleration (Table 1), and we will use Δ_{uz} and α_u throughout to exemplify general patterns.

Plankton likely respond to hydrodynamic signals when these total shears or accelerations exceed detection limits. Although instantaneous signals are difficult to predict, their statistics are easier to characterize, and the frequency of large Δ_{uz} or α_u is related to the signal variances and distribution shape. Assuming that turbulence and wave motions vary independently, they generate signals whose variances are also additive,

$$\sigma_{\Delta_{uz}}^2 = \sigma_{\Delta_{uz}'}^2 + \sigma_{\Delta_{uz}\tilde{u}}^2 \quad (15)$$

$$\sigma_{\alpha_u}^2 = \sigma_{\alpha_u'}^2 + \sigma_{\alpha_u\tilde{u}}^2 \quad (16)$$

where σ is standard deviation and subscripts correspond to the total, turbulence-generated, and wave-generated shears and accelerations. Turbulence generates normally distributed velocities (Mouri et al., 2002), but because turbulence is intermittent, the distribution of velocity gradients can have long, flat tails (high kurtosis; Batchelor, 1953; Van Atta and Antonia, 1980; Gotoh et al., 2002; Beck, 2003). Waves generate surface displacements and velocity gradients that are approximately normally distributed (Massel, 1996; Holthuijsen, 2007). Vorticity is zero under linear surface waves, so the total vorticity is dominated by turbulent motions with a high-kurtosis distribution. The other total signal distributions (Eqs. (15) and (16)) will have shapes most closely resembling those of the dominant signal, affecting the frequency of extreme signal values. For example, at a given shear variance $\sigma_{\Delta_{uz}}^2$, the probability of extreme shears will be higher if fluid motions are dominated by turbulence than if they are dominated by waves. Thus the dominant signal source may be important when fluid motions are weak or when plankton have high detection limits.

The variances of component signals in Eqs. (15) and (16) can be estimated by assuming that turbulence is isotropic at the small scales relevant to plankton (Tennekes and Lumley, 1972) and that waves are governed by linear wave theory (Phillips, 1966). In isotropic turbulence, the variances of shear deformation rates Δ_{uz}' and accelerations α_u' depend on the dissipation rate as

$$\sigma_{\Delta_{uz}'}^2 \approx \frac{\epsilon}{7.5\nu} \quad (17)$$

$$\sigma_{\alpha_u'}^2 \approx a_0 \frac{\epsilon^{1.5}}{\nu^{0.5}} \quad (18)$$

where $a_0 \approx 5$ is the Kolmogorov constant (Taylor, 1935; Voth et al., 2002). In surface gravity waves, energy is distributed across a range of frequencies, and the frequency dependence of the wave amplitudes is described by the sea surface displacement spectrum S . The hydrodynamic signal variances can be estimated as

$$\sigma_{\Delta_{uz}}^2 = \int_0^\infty d\omega k^2 \omega^2 S F' \quad (19)$$

$$\sigma_{\alpha_u}^2 = \int_0^\infty d\omega \omega^4 S F \quad (20)$$

where k is wavenumber ($= 2\pi/\lambda$), computed from frequency using linear wave theory, and F and F' are frequency-dependent structure functions that quantify the vertical decay of wave motions (Table 1; Phillips, 1966). In the absence of spectral data, signal variances can also be estimated using a simpler approximation assuming that all the energy is input at the dominant wave frequency ω_D as

$$\sigma_{\Delta_{uz}}^2 = k^2 \omega_D^2 \frac{H_s^2}{8} F' \quad (21)$$

$$\sigma_{\alpha_u}^2 = \omega_D^4 \frac{H_s^2}{8} F \quad (22)$$

where H_s is the full significant wave height, defined as the mean height of the highest third of waves. The factor of 8 in the denominator arises from assuming that sea surface displacements are normally distributed and assigning all the wave energy to the dominant wave frequency. These equations (Eqs. (17)–(22)) provide a means of estimating the velocity gradients that plankton experience directly, which are rarely reported in observational studies, from a small set of environmental variables that are measured and reported more frequently.

2.4. Hydrodynamic forces on plankton

Hydrodynamic signals can be extrapolated directly to behavior in only a handful of species whose responses to flow have been thoroughly characterized (e.g., Latz et al., 1994; Kiørboe et al., 1999; Latz and Rohr, 1999; Fuchs et al., 2013; Fuchs et al., 2015b). Although shears or accelerations are the ultimate inducers of a behavioral response, sensing occurs through a proximate mechanism of fluid forces that bend, stretch, or deform a sensory receptor (e.g., Gillespie and Walker, 2001; Echevarria et al., 2014; Tesson and Latz, 2015). For example, a copepod would sense a linear velocity gradient du/dz that creates sufficient spatial variation in the drag force to bend the external sensory setae, inducing a neurophysiological signal (Gill and Crisp, 1985; Yen et al., 1992). Similarly, an oyster larva can sense a velocity gradient that induces sufficient torque to rotate the larvae and induce motion of a statolith, bending the sensory hair cells within the statocyst lumen and transmitting a nerve impulse (Gallin and Wiederhold, 1977; Chia et al., 1981; Fuchs et al., 2015b). Unlike shears and accelerations, fluid forces on a plankter depend on organismal characteristics such as size, mass, and swimming speed. To generalize how plankter characteristics affect flow sensitivity, it is useful to

conceptualize hydrodynamic signals in terms of the forces exerted on plankton.

Some forces affect motion even in the absence of flow and depend on a plankter's mass, shape, or behavior. For example, if an organism swims or sinks, its motion is retarded by an opposing drag force

$$F_d = \frac{1}{2} \rho_f A C_d \mathbf{u}_s^2, \quad (23)$$

where ρ_f is fluid density, A is projected area of the organism, C_d is a drag coefficient, and \mathbf{u}_s is swimming or sinking speed relative to the water, where bold indicates a vector (e.g., Vogel, 1994). The drag coefficient encompasses contributions from both viscous forces (Stokes drag) and inertial forces (form drag). The relative contributions of Stokes drag and form drag depend on the Reynolds number of flow immediately around an organism, $Re_p = u_s d / \nu$ where d is the organism's length or diameter. At $Re_p < 1$ inertial forces are small, the viscous drag dominates, effects of shape on drag are negligible, and the drag coefficient is $C_d = 24/Re_p$ (Clift et al., 1978). Many plankton fall in this category and can be treated as spherical with radius r , simplifying Eq. (23) to

$$F_d = 6\pi r \rho_f \nu \mathbf{u}_s \quad (24)$$

This Stokes drag is caused primarily by skin friction on the body's surface and can be thought of as a baseline level of mechanical stimulus.

Fluid motion exerts additional forces that may be experienced by plankton as a hydrodynamic signal, and these forces can be tangential or normal to a surface. Tangential forces are due to shear stress on an organism's surface and are proportional to the intensity of mechanical deformation of the body wall (e.g., Latz et al., 1994). Shear stress is a force per unit area, $\tau = F_s/A$, and is typically defined as $\tau = \nu \rho_f du/dz$. By combining these two relations, we can express the tangential force on a body as

$$F_s = \nu \rho_f A \frac{du}{dz}. \quad (25)$$

This "shear force" is a simplified approximation of the tangential force from shear-induced added drag (Rubinow and Keller, 1961; Saffman, 1965; Kurose and Komori, 1999). Fluid motions also exert normal forces due to longitudinal deformation (e.g., du/dx) that would stretch or compress a plankter. These signals are smaller than those due to shear deformation (Table 1), and the mechanisms of stretch- or compression-sensing are unknown (e.g., Stake and Sammarco, 2003; Fraser, 2006), so here we focus on the tangential shear force.

The shear force creates a mechanical deformation through relative motion of fluid past the organism, like the viscous drag force but with two caveats. First, the viscous drag force F_d is oriented opposite to any swimming or sinking motion, whereas the shear force F_s orientation depends on flow direction relative to the body. Second, small-scale velocity gradients are approximately linear (Lazier and Mann, 1989), and the shear force can have different signs on opposite sides of a suspended body. This asymmetry induces a viscous torque that rotates a plankter. At equilibrium, the angle of rotation ϕ is determined by a balance of the viscous torque and the gravitational torque created by an offset in the centers of gravity and buoyancy,

$$\sin \phi = \frac{3\nu \rho_f \xi}{L \rho_p g}, \quad (26)$$

where ξ is vorticity, L is the distance between the body's centers of buoyancy and gravity, ρ_p is the plankter density, and g is the acceleration due to gravity (Kessler, 1986; Jonsson et al., 1991). The distance L can be estimated from the body orientation in laminar shear

or rotating flow but is typically a small percentage of the body length ($L < 0.03d$; Kessler, 1986; Jonsson et al., 1991). Organisms that are more dense or have a more asymmetric density distribution are more resistant to shear-induced rotation (Mogami et al., 2001; Grünbaum and Strathmann, 2003) and may sense the shear force mainly as a deformation using external mechanosensors such as antennae. In contrast, neutrally buoyant, symmetric organisms are more prone to shear-induced rotation (Karp-Boss and Jumars, 1998; Guasto et al., 2012) and may sense the shear force mainly as a change in orientation using internal gravity-detectors such as statocysts.

Plankton also experience normal forces due to pressure gradients generated by fluid acceleration. The pressure gradient force is

$$F_a = \frac{4}{3} \pi r^3 \rho_f \frac{d\mathbf{u}}{dt}, \quad (27)$$

where \mathbf{u} is the fluid velocity vector and its derivative is taken following a particle's trajectory (Maxey and Riley, 1983; Mei, 1996). Unlike the shear force, which can mechanically deform and rotate a plankter, the pressure gradient force accelerates the whole organism and contributes to its overall motion. These acceleration-induced motions likely would be sensed with internal motion detectors functioning as accelerometers. Both accelerations and shear-induced rotations could be detected with internal sensors such as statocysts (Fuchs et al., 2015b,a), while shear forces could be sensed with internal or external receptors depending on the body's orientational stability (e.g., Kjørboe et al., 1999; Fuchs et al., 2015a). For simplicity, we use the shear force F_s and pressure gradient force F_a to summarize the intensity of hydrodynamic signals that plankton would sense with different receptor types.

3. Methods

We examined how turbulence- and wave-generated signals vary among seascapes using three types of data: published dissipation rates and wave statistics, publicly available buoy data from the National Data Buoy Center (NDBC), and re-analyzed observations of turbulence and waves from two coastal sites. Most NDBC data were taken from discus and waverider buoys. Both buoy types provide historical data archived as annual records of basic wave data, including significant wave height and dominant wave period, that can be used to characterize wave-generated velocity gradients. Discus buoys also provide more recent, shorter (45-day) records of real-time data that have undergone fewer quality-control steps but include wind speed and wind-wave height, suitable for estimating dissipation rates and velocity gradients generated by both waves and turbulence. A synthesis of multiple data types enabled us to characterize the spatially varying intensity of turbulence and wave motions and to quantify the statistics of shears, accelerations, and hydrodynamic forces experienced by plankton in different seascapes.

3.1. Spatial variation in turbulence

We characterized the intensity of turbulence in different seascapes by compiling published dissipation rates and by estimating dissipation rates from buoy data (Fig. 2). The published data are consolidated from diverse observations in each seascape type, including recent measurements near the surface and bottom boundaries and under breaking waves (see Appendix, Table A.1). The data represent a wide range of forcing conditions and stratification. The references are nonexhaustive, and we omit observations made exclusively below the mixed layer where plankton are sparse (e.g., Whalen et al., 2012) and instantaneous measurements reported without spatial or temporal averaging



Fig. 2. Google map of buoys and study sites used in data compilation. Some symbols overlap.

(Gemmrich and Farmer, 2004; Gemmrich, 2010). We also used subsets of some data to estimate the ranges of dissipation rates within the upper and lower 2 m of the water column, representing the most energetic parts of the SBL and BBL. Ranges of dissipation rates were taken from the text or estimated by eye from figures, and clear outliers were omitted. We estimated the mean dissipation rate on a \log_{10} scale from tabular values or histograms where possible, or as the center of the observed range of $\log_{10}\varepsilon$, assuming that dissipation rates are lognormally distributed (Kolmogorov, 1962). Although the lognormal assumption is sometimes invalid for measurements in the mixed layer (Yamazaki and Lueck, 1990), it often provides accurate estimates of central tendency (Gregg et al., 1986; Moum et al., 1995). We used these estimates of mean $\log_{10}\varepsilon$ to represent the range of dissipation rates that occur frequently in a seascape type.

Until recently, dissipation rates have rarely been measured in wave-affected surface waters where direct observations are difficult, so to fill this gap we also estimated dissipation rates in the upper water column using NDBC buoy data (see Appendix, Table A.2). We estimated ε as

$$\varepsilon = \max[\varepsilon_w, \varepsilon_r] \quad (28)$$

where ε_r and ε_w are given by Eqs. (1), (2). The shear velocity was calculated from the wind stress τ estimated as

$$u_*^2 = \frac{\tau}{\rho_f} = C_d U_w^2 \frac{\rho_a}{\rho_f} \quad (29)$$

where $C_d = 1.15 \times 10^{-3}$ is a drag coefficient, U_w is wind speed at 10 m, and ρ_a is air density (e.g., Smith, 1980). The transfer velocity c_e in Eq. (2) was estimated from the wind speed as

$$c_e = a_0 U_w + a_1 \quad (30)$$

where $a_0 = 0.148$ and $a_1 = 1.11 \text{ m s}^{-1}$ are empirical constants (Hwang, 2009). Wind speeds U_w and wind-wave heights H_w were taken from 45-day records of real-time data from discus buoys, and wind speeds were corrected from the recording height of 5 m to 10 m using the wind profile power law (Peterson and Hennessey, 1978). The observation period (19 April–3 June, 2014) excludes the windier winter months but spans a productive time for plankton. For each buoy data set, ε was calculated for all recorded time points from $z = 20 \text{ m}$ below the surface to $H_w/2$, the maximum height at which Eq. (2) can be considered valid (Terray et al., 1996). As with the published dissipation rate estimates, we recorded the range of values and the center of the range of $\log_{10}\varepsilon$. These buoy estimates supplement the published observa-

tions and extend the estimated range of dissipation rates in the wave-affected surface layer.

3.2. Spatial variation in waves

To characterize the variation of wave-generated signals in different seascapes, we analyzed wave statistics from historical NDBC buoy data and from the literature. The NDBC historical data (see Appendix, Table A.2) include the dominant wave period ω_D and significant wave height H_s but no spectral data. We used the most recent 5 years of archived data through 2013 and the approximations in Eqs. (21), (22) to estimate wave-generated shear and acceleration variances, $\sigma_{\Delta_{uz}}^2$ and $\sigma_{\bar{u}_i}^2$, as monthly averages over a depth range of $z = 20 \text{ m}$ to $H_s/2$ below the surface. Buoy records of ω_D and H_s are lacking for sheltered inlets and estuaries and for the surf zone. For these shallow seascapes, we estimated wave-generated signals by computing $\sigma_{\Delta_{uz}}^2$ and $\sigma_{\bar{u}_i}^2$ from observations of ω_D and H_s reported in the literature (Table 2). These estimates rely on linear wave theory and are speculative in the surf zone, where waves are highly nonlinear. We recorded the range of standard deviations (SD) $\sigma_{\Delta_{uz}}$ and $\sigma_{\bar{u}_i}$ and used the \log_{10} -scale means of these estimates to represent the range of wave-generated signals that occur frequently in each seascape.

3.3. Combined turbulence- and wave-generated signals

Plankton experience the total shears and accelerations produced by turbulence and waves as they co-occur, so we quantified these simultaneous signals using coastal observations and NDBC buoy data. We analyzed the co-occurring hydrodynamic signals in sheltered versus exposed habitats using data from two sites in Massachusetts, United States: a sheltered, well-mixed tidal inlet (BH; Barnstable Harbor) and an exposed site on the inner shelf (MVCO; Martha's Vineyard Coastal Observatory). The observations at BH were collected in the navigational channel during July 2004 using an acoustic Doppler velocimeter (ADV) that measured at 0.78 m above the bottom in a mean depth of 6.8 m (Fuchs et al., 2010). The observations at MVCO were made during the CBLAST study in the fall of 2003 using several ADVs that measured at a depth of about 2 m below the mean sea surface in 16 m water depth (Gerbi et al., 2009). These two data sets represent different boundary layers but enable a detailed comparison of sheltered conditions, where waves are generated only by the local winds, versus exposed conditions, where waves can include both locally-generated wind waves and swell.

Table 2

Summary of typical wave statistics, including full significant wave height H_s , dominant wave period T_D , and water depth h used to estimate wave-generated signals for each seascape type. Literature values are given as a range of estimates. Values for continental shelf and open ocean are the mean and range of monthly means over all NDBC buoys within a seascape/ocean from most recent five years of historical data through 2013 (see Appendix, Table A.2).

Seascape	Ocean	H_s (m)	T_D (s)	h (m)	References	
Surf zone	Atlantic	0.7–1.2	9–10	3.2	Fedderson et al. (2007)	
	Pacific	0.6–0.95	13–17	1.3–1.6	Elgar et al. (1988)	
Estuaries and inlets	Small fetch (<20 km)	Atlantic	2.4–3.0	<5	Jackson and Nordstrom (1992)	
			0.09–0.14	2.1–2.2	<6	Sherman et al. (1994)
	Large fetch (>20 km)	Atlantic	0.13–0.21	2.7–3.0	<5	Jackson and Nordstrom (1992)
			0.12–0.20	2.8–3.4	<6	Jackson and Nordstrom (1994)
		Pacific	0.09–0.2	2.5–9.1	4	Jackson (1995)
			0.15–0.21	2.9–3.1	4.4–10.9	Stevens and Lacy (2012)
Continental shelf	Atlantic	1.1 (0.4–2.8)	7.1 (4.0–10.1)	59 (10–206)	NDBC data	
	Pacific	1.8 (0.6–3.2)	11.4 (8.4–13.5)	122 (19–363)	NDBC data	
Open ocean	Atlantic	1.9 (1.1–2.6)	8.9 (7.0–10.7)	4830 (3485–5515)	NDBC data	
	Pacific	2.6 (1.5–4.4)	10.5 (8.2–13.1)	4219 (3440–4755)	NDBC data	

For each coastal site we estimated the turbulence-generated, wave-generated, and total velocity gradients. We computed the variances of turbulence-generated shears and accelerations ($\sigma_{\Delta_{uz}}^2$ and $\sigma_{\alpha_{uz}}^2$) from dissipation rates (Eqs. (17) and (18)). At BH the near-bed velocity record showed little evidence of waves, so dissipation rates were estimated using the inertial subrange of the ADV vertical velocity spectrum (Fuchs et al., 2010). At MVCO wave activity made spectral estimates of dissipation rate difficult, so dissipation rates were estimated from measured wind stress and H_w using Eq. (2) (Churchill et al., 2006; Gerbi et al., 2009). At both sites we computed the variances of wave-generated shear and acceleration ($\sigma_{\Delta_{uz}}^2$ and $\sigma_{\alpha_{uz}}^2$) from the wave spectrum using ADV vertical velocity time series and linear wave theory (Eqs. (19) and (20)). At MVCO, we also computed the wave-generated signal variances using the significant wave height and dominant wave period (Eqs. (21) and (22)) solely for comparison to the spectral estimates (Eqs. (19) and (20)). We did not do this comparison for BH because waves were weak, particularly in the near-bed location of our observations. Finally, we calculated the total variances of signals $\sigma_{\Delta_{uz}}^2$ and $\sigma_{\alpha_{uz}}^2$ at each site using Eqs. (15) and (16). The signal distributions at these two sites exemplify how turbulence and waves influence seascape characteristics in sheltered inlets and on the continental shelf.

To compare how hydrodynamic signals co-vary on the continental shelf and open ocean, we similarly analyzed real-time NDBC data from discus buoys that include both standard meteorology and wave spectral data. For each 45-day buoy record, we estimated the turbulence-generated signal variances ($\sigma_{\Delta_{uz}}^2$ and $\sigma_{\alpha_{uz}}^2$) from time- and depth-averaged dissipation rates, which were estimated using Eqs. (17) and (18) (Section 3.1). We estimated the wave-generated signal variances ($\sigma_{\Delta_{uz}}^2$ and $\sigma_{\alpha_{uz}}^2$) from the time-averaged significant wave height and dominant wave period using Eqs. (21) and (22). Finally we computed the total variances of signals $\sigma_{\Delta_{uz}}^2$ and $\sigma_{\alpha_{uz}}^2$ using Eqs. (15) and (16). These signal estimates from buoy data provide insight on the relative influence of turbulence and waves among exposed habitats that vary in their water depth and fetch.

Multiple estimates were condensed to define the ranges of co-occurring hydrodynamic signals that occur frequently and can be considered typical of each habitat type. For each seascape we defined frequently-occurring dissipation rates as those within the range of \log_{10} -scale mean ε from observations and buoy estimates. These frequently-occurring dissipation rates were used to estimate the range of frequently-occurring, turbulence-generated signal

variances ($\sigma_{\Delta_{uz}}^2$ and $\sigma_{\alpha_{uz}}^2$), assuming that turbulence is isotropic (Eqs. (17) and (18)). For each seascape we defined frequently-occurring wave conditions by the range of \log_{10} -scale mean wave-generated signals ($\sigma_{\Delta_{uz}}^2$ and $\sigma_{\alpha_{uz}}^2$) estimated from buoy and literature data (Eqs. (21) and (22); Section 3.2). Lastly, in each seascape we estimated the total signal variances ($\sigma_{\Delta_{uz}}^2$ and $\sigma_{\alpha_{uz}}^2$) by summing the variances of turbulence- and wave-generated signals produced over all frequently-occurring turbulence and wave conditions (Eqs. (15) and (16)). This approach assumes that turbulence and waves are uncorrelated and is invalid in the surf zone, but in the absence of a more appropriate theory we treated all seascapes equally. These total signal variances describe a general pattern of how velocity gradients covary among seascapes and are defined hereafter as typical signals in each seascape.

3.4. Relating signals to sensing and forces on plankton

We related the typical hydrodynamic signals to observed plankton behaviors using three exemplary species with different sizes, receptor types, and behavioral responses. Dinoflagellates bioluminesce at high shear stress (e.g., Latz et al., 1994; Latz and Rohr, 1999; Latz et al., 2004), sensing shear as deformation of the cell wall. *Ceratocorys horrida* ($d = 70 \mu\text{m}$) is the most sensitive species observed and produces bioluminescent flashes in laminar pipe flow with wall stress of $\geq 0.02 \text{ N m}^{-2}$ (Latz et al., 2004). Some invertebrate larvae change their vertical motions in response to turbulence (e.g., Young, 1995; Welch and Forward, 2001; McDonald, 2012), and behaviors are most thoroughly characterized for oysters, *Crassostrea virginica*. Pediveliger larvae ($d \approx 310 \mu\text{m}$) sense flow using statocysts and either swim faster upward or actively dive in response to accelerations of $\geq 1 \text{ m s}^{-2}$ or to body rotations induced by turbulent vorticity of $\geq 0.4 \text{ s}^{-1}$ (Fuchs et al., 2013; Fuchs et al., 2015b; Fuchs et al., 2015a). Some copepods perform escape jumps in shear or turbulence (reviewed by Kiørboe, 2011; Buskey et al., 2012), and behaviors are most often studied in *Acartia tonsa*. The adults ($d \approx 900 \mu\text{m}$) sense shear as bending of mechanosensory setae on the antennae and jump at above-threshold deformations, although the threshold varies with experimental conditions (Kiørboe et al., 1999; Gilbert and Buskey, 2005; Webster et al., 2015). Each study quantified a different type of shear, so we converted all shears to dissipation rates using turbulence equations (Table 1) or used the authors' estimates of threshold dissipation rate.

We also used the co-occurring shears and accelerations to generalize the typical forces exerted by fluid motion on plankton in

Table 3
Representative plankton and their length scales d and swimming speeds u_s .

Taxon	d (μm)	u_s (cm s^{-1})	Reference
Dinoflagellates			
Various	15–58	0.01–0.06	Kamykowski and McCollum (1986)
Various	15–48	0.01–0.03	Kamykowski et al. (1992)
<i>Alexandrium</i> spp.	22–41	0.003–0.04	Lewis et al. (2006)
Ciliates			
<i>Uronema</i>	25	0.12	Sleigh and Blake (1977)
<i>Paramecium</i>	210	0.1	Sleigh and Blake (1977)
Invertebrate larvae			
<i>Bugula</i> spp.	160–270	0.3–0.5	Wendt (2000)
<i>Crassostrea virginica</i>	320	0.02	Fuchs et al. (2013)
<i>Philine aperta</i>	150–390	0.15	Hansen (1991)
<i>Ilyanassa obsoleta</i>	590–770	0.08–0.4	Fuchs et al. (2004)
Copepods			
<i>Calanus pacificus</i>	220–3000	0.03–0.7	Greene et al. (1986)
<i>Paracalanus parvus</i>	670	0.06	Tiselius and Jonsson (1990)
<i>Pseudocalanus elongatus</i>	920	0.05	Tiselius and Jonsson (1990)
<i>Centropages typicus</i>	1300	0.19	Tiselius and Jonsson (1990)
<i>Centropages hamatus</i>	1030	0.72	Tiselius and Jonsson (1990)
<i>Euchaeta rimana</i>	2500	0.7	Yen (1988)

different seascapes. Forces on a plankter vary with its size and swimming speed, so we used idealized examples of three sizes: $d = 30 \mu\text{m}$ representing dinoflagellates and small ciliates, $d = 200 \mu\text{m}$ representing larger ciliates and small invertebrate larvae, and $d = 1000 \mu\text{m}$ representing larger invertebrate larvae and small copepods (Table 3). For each organism we estimated the shear force F_s by substituting $\sigma_{\Delta u_z}$ for du/dz in Eq. (25) and estimated the pressure gradient force F_a by substituting σ_{z_u} for $d\mathbf{u}/dt$ in Eq. (27), using the ranges of $\sigma_{\Delta u_z}$ and σ_{z_u} that were typical in each seascape. These estimates of F_s and F_a are calculated from the typical signals and represent standard deviations of the magnitude of shear forces and pressure gradient forces, respectively. The shear force likely must exceed the viscous drag to be sensed by a swimming organism, so we also calculated the viscous drag F_d (Eq. (24)) for a range of swimming speeds ($u_s = 0.01, 0.1,$ and 1.0 cm s^{-1}) to provide estimates of the minimum detectable shear force. The shear force and pressure gradient force represent signals that could be sensed with different receptor types and provide insight into how sensitivity to shears and accelerations might vary among taxa and among ocean regions.

4. Results

4.1. Spatial variation in turbulence

The seascape regions that we examined had broad ranges of observed dissipation rates with considerable overlap (Fig. 3A, references in Table A.1). The ranges of ε observed in individual studies were smaller than the full range of ε observed in aggregate within a seascape type by one to several orders of magnitude. Estimates from buoy data were more consistent within seascapes and typically ranged from $\varepsilon \approx 10^{-9.5} - 10^{-4.5} \text{ m}^2 \text{ s}^{-3}$ (Fig. 3B). This consistency reflects the fact that buoy estimates of ε all spanned the same date range and the same depth range (≤ 20 mbs), including near-surface estimates that are missing from most observations. Buoy estimates suggest that mixed-layer dissipation rates are well represented by observations on the continental shelf but not in the open ocean, where microstructure observations typically omit the upper 5–10 m. The largest dissipation rates were observed in surface and bottom boundary layers. Although SBL observations were sometimes large in all locations, the BBL in estuaries and inlets was generally more turbulent than the BBL on the continental shelf (Fig. 4). This result reflects the

fact that bottom currents are strongest in shallow water. The range of frequently occurring ε was defined here by the \log_{10} -scale means from all dissipation estimates (Fig. 3). Using this metric, the maximum frequently occurring ε differed by a factor of ≤ 2 among inlets and estuaries, continental shelves, and the open ocean, but was ~ 100 times larger in surf zones than in other seascapes.

4.2. Spatial variation in waves

Spatial patterns were more evident in the wave-generated accelerations estimated from buoy and literature data (Fig. 5). Acceleration ranges were seascape-specific due to geographic variation in the significant wave height and dominant wave period (Table 2, Fig. 5). Average significant wave heights in the open ocean were nearly double those on the continental shelf, and wave-generated accelerations were frequently higher in the open ocean than on the shelf. Of the shallow seascapes, estuaries and inlets had the smallest wave heights and shortest periods, corresponding to the smallest wave-generated accelerations. Surf zones had intermediate wave heights but long wave periods similar to those on the continental shelf and open ocean (Table 2). The estimated wave-generated accelerations in the surf zone were comparable to the maximum estimates in other seascapes, although in the surf zone measurements are scarce and theory is uncertain. Overall the frequently-occurring, wave-generated accelerations were highest in the surf zone, followed by the open ocean, continental shelves, and sheltered coastal sites.

These indirect estimates, computed from buoy records or literature values of H_s and ω_D , were generally comparable to the few available direct observations of wave-generated accelerations (Fig. 5). The buoy-based estimates from the continental shelf spanned a range similar to the observed wave-generated accelerations at MVCO (Fig. 5A and B). The literature-based estimates for estuaries also spanned a range similar to the observed wave-generated accelerations at BH (Fig. 5A). The BH observations had a lower mean value than the literature-based estimates due to differences in morphology and methodology: BH has a shorter fetch (~ 6 km channel) than the other estuaries (Table 2), and observations at BH were made near the seabed where waves are weakest, whereas the indirect estimates of accelerations were computed over the whole water depth. In the surf zone, the only available observations are of total accelerations (Elgar et al., 1988; Elgar

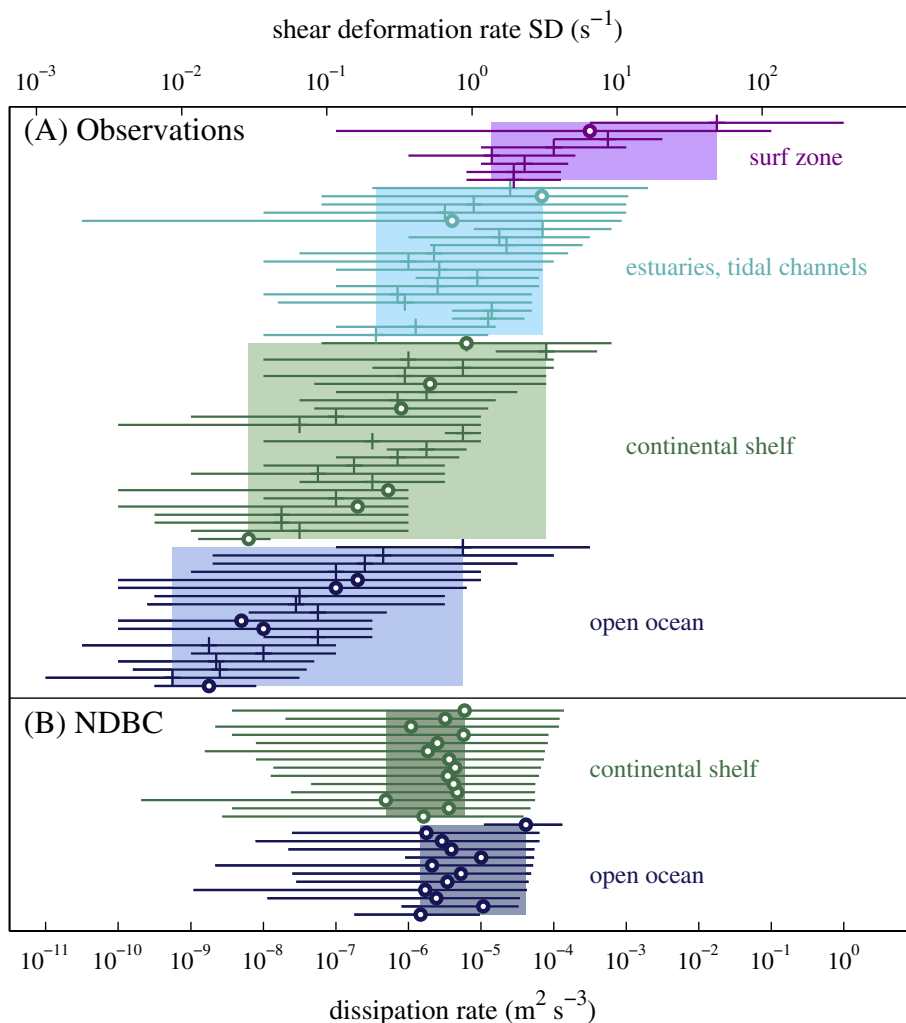


Fig. 3. Ranges of dissipation rates ε (bottom axis) and corresponding shear deformation rate $SD \sigma'_{\Delta z}$ (top axis): (A) from observations and (B) estimated from NDBC buoy data. Solid lines are ranges of minimum to maximum values observed (A) or estimated in the upper 20 m using monthly-averaged wind data (B). Circles mark \log_{10} -scale mean ε where available, and + marks center of \log_{10} -scale ε distribution from field studies where no means were available. Shaded areas represent range of \log_{10} -scale mean ε estimates for each seascape type. Colors indicate the surf zone (magenta), inlets and estuaries (cyan), continental shelf (green), and open ocean (blue). Each line represents a different set of observations or buoy (see Appendix, Tables A.1 and A.2); some field studies report ranges for multiple depths.

et al., 1990). The literature-based estimates of wave-generated accelerations are within the range of the observed total accelerations (Fig. 5A), suggesting that our surf-zone estimates of wave-generated signals are on the correct order.

4.3. Combined turbulence- and wave-generated signals

The total shears and accelerations include contributions from both turbulence and waves, which differed in their relative influence on hydrodynamic signals at the sheltered and exposed coastal sites (Fig. 6). The temporal variation of shears and accelerations was dominated by tidal currents at the near-bed BH site and by weather at the near-surface MVCO site (not shown). The sheltered BH site had strong turbulence but minimal waves, and the accelerations due to waves exceeded those due to turbulence only at slack tides. The wave signal was small both because BH is sheltered with a short fetch and because observations were collected near the bottom. The distributions of both total shear and total acceleration were dominated by turbulence. The exposed MVCO site had weaker turbulence but larger wind-generated waves and swell, and while the total shear distribution was dominated by turbulence, the total acceleration distribution was dominated by waves.

These results illustrate the potential for hydrodynamic signals to be controlled by different physical processes in different habitat types.

We also used the MVCO data to compare the spectral estimates of wave-generated shears and accelerations (Eqs. (19) and (20)) against the simpler estimates computed from the dominant wave characteristics (Eqs. (21) and (22)). The simpler functions underestimated the wave-generated shears but gave good estimates of wave-generated accelerations (Fig. 7). This difference may reflect the stronger dependence of shears on frequency; $k \propto \omega^2$ in deep water, so the shears scale with $\sim \omega^6$, whereas the accelerations scale with $\sim \omega^4$, making the shears more sensitive to the exclusion of high frequencies in Eqs. (21) and (22). We are confident that the underestimates of wave-generated shears should contribute little error to estimates of total shears, because the spectral estimates confirm that the generation of shears is generally dominated by turbulence (Fig. 6).

In all seascapes the typical shears were primarily generated by turbulence, while the typical accelerations were primarily generated by waves (Fig. 8, Table 4). At most dissipation rates ($\varepsilon \geq 10^{-8} \text{ m}^2 \text{ s}^{-3}$) and all typical wave conditions, the variance of total shear deformation rate was entirely determined by

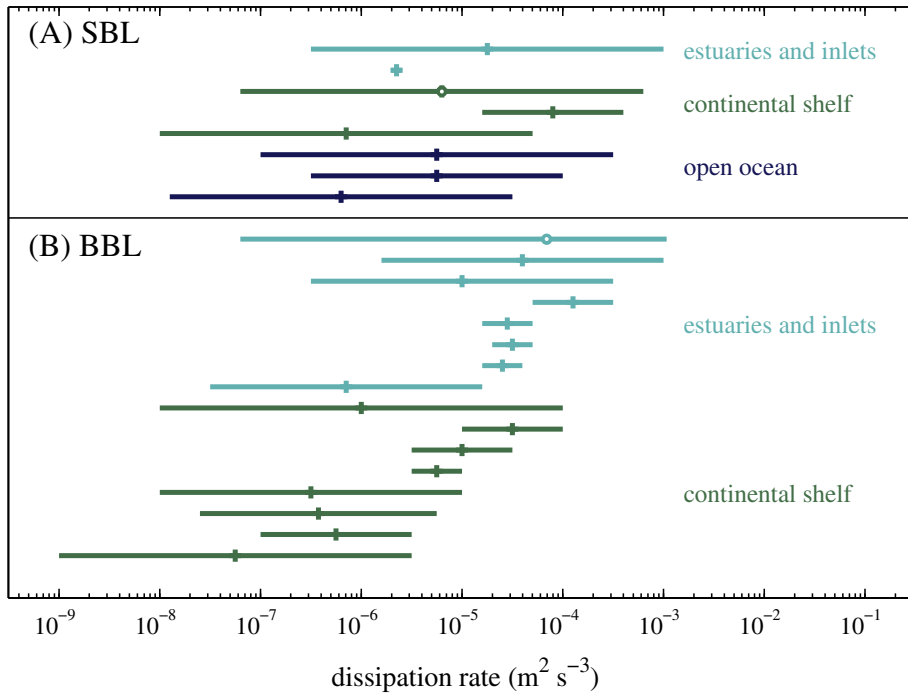


Fig. 4. Ranges of dissipation rate from boundary-layer observations: (A) in the surface boundary layer (SBL) between 0 and 2 m below surface and (B) in the bottom boundary layer (BBL) between 0 and 2 m above bottom. Colors, lines, and symbols as in Fig. 3. Observations are a subset of those in Fig. 3A.

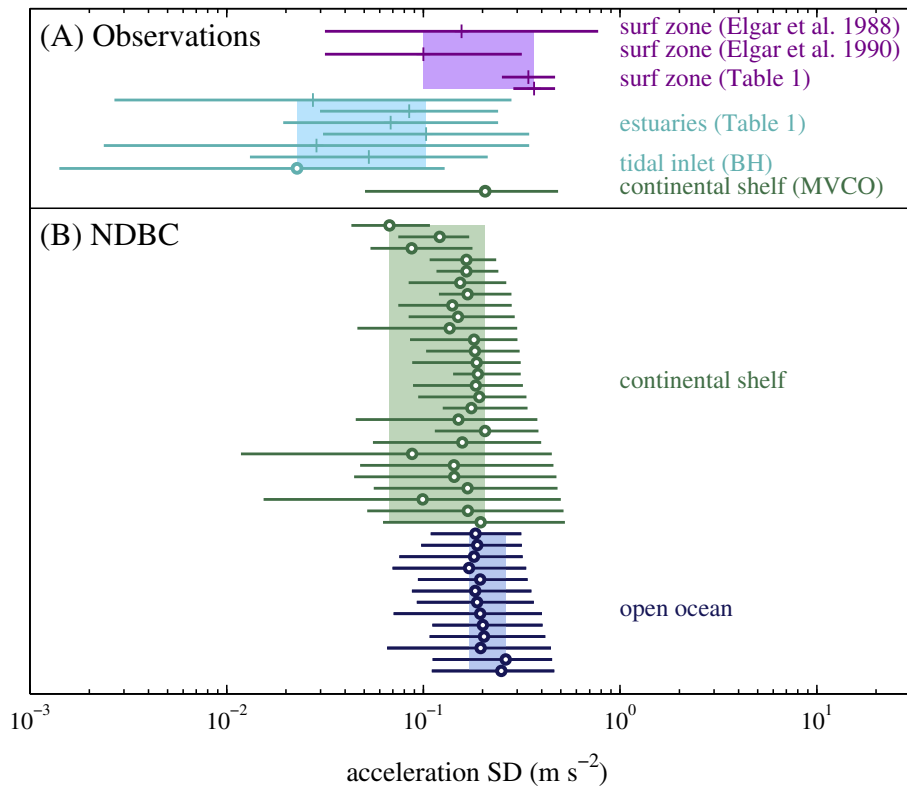


Fig. 5. Ranges of wave-generated acceleration SD σ_a : (A) from observations or estimated from literature data and (B) estimated from NDBC buoy data. All wave-generated accelerations were estimated from significant wave height H_s and dominant wave period ω_D ; Elgar et al. (1988, 1990) report total accelerations. Colors, lines, and symbols as in Fig. 3. Each line represents a different set of observations (see text; Table 2) or buoy (see Appendix, Table A.2). Shaded areas represent ranges of \log_{10} -scale mean σ_a estimates from each seascape.

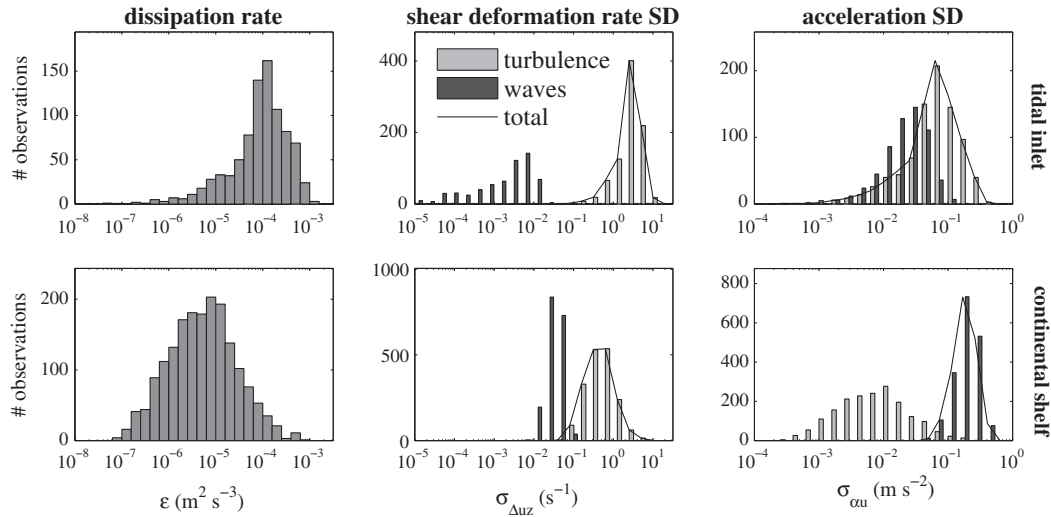


Fig. 6. Histograms show dissipation rate ϵ (left), shear deformation rate SD $\sigma_{\Delta u}$ (center), and acceleration SD σ_{a_u} (right) due to turbulence (light gray), waves (dark gray), and both processes combined (black line) in a well-mixed tidal inlet at Barnstable Harbor, MA (upper; Fuchs et al., 2010) and on the continental shelf at Martha’s Vineyard Coastal Observatory (lower; Gerbi et al., 2009). Wave-generated signals are spectral estimates (Eqs. (19) and (20)).

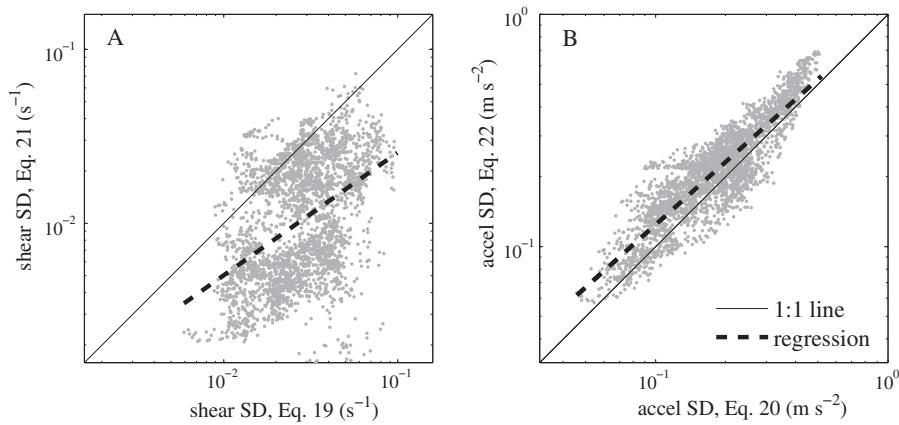


Fig. 7. A comparison of shear SD (A) and acceleration SD (B) computed from spectral estimates (Eqs. (19) and (20); x-axes) and from dominant wave characteristics (Eqs. (21) and (22); y-axes) at MVCO. Solid lines are 1:1, dashed lines are log₁₀-scale linear regressions ($R^2 = 0.18$, $p = 0.11$ for shear, and $R^2 = 0.80$, $p = 0.01$ for acceleration).

turbulence (Fig. 8A) and was largest in shallow regions where turbulence is strong near both boundaries. This pattern would be echoed in other forms of spatial velocity gradients including vorticity, which is zero under linear surface waves. In contrast, at most dissipation rates ($\epsilon \leq 10^{-3} \text{ m}^2 \text{ s}^{-3}$) the variance of total acceleration was strongly influenced by waves (Fig. 8B) and generally was larger in offshore regions where winds are strong and the fetch is unlimited. The largest dissipation rates ($\epsilon > 10^{-3} \text{ m}^2 \text{ s}^{-3}$) occurred frequently only in the surf zone, which was the only location where accelerations were dominated by turbulence rather than by waves under more energetic conditions. These results agree with predictions of where turbulence should dominate the production of shears or accelerations (Eqs. (10) and (11), Section 2.2) and demonstrate that the dissipation rate is generally a good predictor of shear magnitudes but a bad predictor of acceleration magnitudes.

The relative influence of turbulence and waves was reflected in the joint distributions of typical shears and accelerations, which demarcated seascapes as distinct hydrodynamic environments (Fig. 9). The surf zone contained the largest signals of both types and had little overlap with signal ranges in other seascapes. The

continental shelves and open ocean were most hydrodynamically similar to each other and shared similar ranges of shears and some overlap in accelerations. The open ocean and inlets and estuaries were completely distinct from each other due to differences in their ranges of typical accelerations. Despite considerable overlap in shear distributions, all seascapes exhibited some range of joint signal distributions that was unique.

The typical signal ranges generally agreed with individual estimates of co-occurring $\sigma_{\Delta u}$ and σ_{a_u} from real-time buoy data and coastal data sets (Fig. 9). Estimates from real-time buoy data fell within the typical signal range on the continental shelf but not in the open ocean, where some real-time buoy estimates had accelerations lower than the typical range. This difference indicates that the spring real-time data lacked the larger sea states present in the fall and winter months that are included in historical data. On the continental shelf, the MVCO observations spanned the full range of typical signals and beyond; this additional scatter reflects the fact that mean estimates at MVCO were at the high end of those used to calculate typical signals, partly because MVCO data are from the surface boundary layer, whereas the indirect estimates extend to 20 m depth. The least

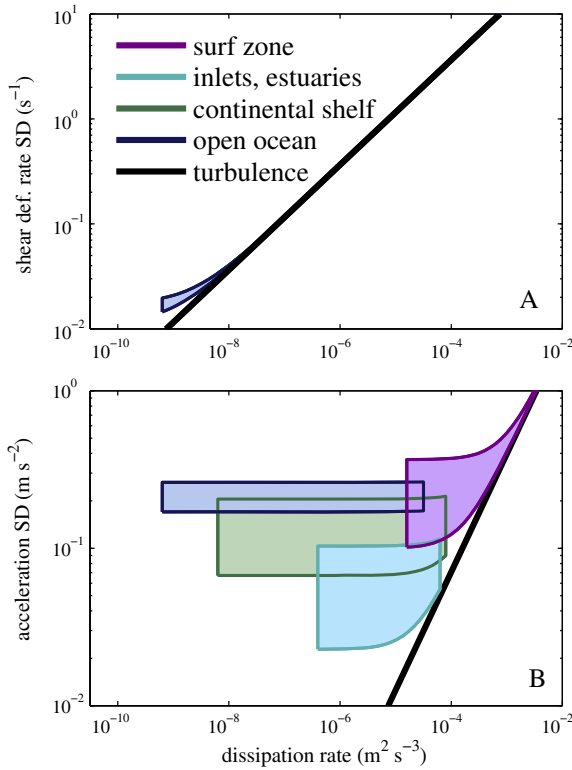


Fig. 8. Ranges of typical hydrodynamic signals in different seascapes: (A) shear deformation rate SD $\sigma_{\Delta_{uz}}$ and (B) acceleration SD σ_{α_u} vs. dissipation rate ϵ . Black solid line represents signal distributions in isotropic turbulence. Color patches represent total signal distributions caused by isotropic turbulence plus waves (Eqs. (15) and (16)), computed over the range of frequently occurring turbulence and wave-generated signals in each seascape (Figs. 3 and 5). Colors as in Fig. 3. Color patches for shear in surf zones, inlets and estuaries, and continental shelves (A) cannot be seen because total shear variances are dominated by turbulence at frequently occurring dissipation rates. Color patch for acceleration in surf zone (B) curves upward because total acceleration variances are dominated by waves at lower dissipation rates and by turbulence at higher dissipation rates.

agreement was seen between BH observations and the estimated ranges of typical signals in inlets and estuaries. The BH data fell almost entirely on the expected signal distribution for isotropic turbulence and had shears extending into the typical range for the surf zone. The near-bed measurement location and the short fetch of the BH inlet make these observations more representative of nearshore BBLs than of an average estuarine water column.

4.4. Sensing and forces on plankton

Three species were used to exemplify how the threshold signals for observed plankton behaviors compare to typical signal ranges

Table 4
Ranges of standard deviations for typical hydrodynamic signals in four seascapes, including turbulence-generated, wave-generated, and total signals. See Table 1 for definitions.

Signal	Source		Surf zone	Inlets & estuaries	Continental shelf	Open ocean
Shear deformation rate (s^{-1})	Turbulence	$\sigma_{\Delta'_{uz}}$	1–40	0.2–3	0.03–3	0.01–2
	Waves	$\sigma_{\Delta_{uz}}$	0.07	0.002–0.03	0.003–0.02	0.01–0.02
	Total	$\sigma_{\Delta_{uz}}$	1–40	0.2–3	0.03–3	0.01–2
Vorticity (s^{-1})	Turbulence	$\sigma_{\zeta'}$	2–80	0.3–5	0.05–5	0.01–4
	Waves	σ_{ζ}	0	0	0	0
	Total	σ_{ζ}	2–80	0.3–5	0.05–5	0.01–4
Acceleration ($m\ s^{-2}$)	Turbulence	$\sigma_{\alpha'_u}$	0.02–2	0.001–0.04	10^{-4} –0.06	10^{-6} –0.03
	Waves	σ_{α_u}	0.1–0.4	0.02–0.1	0.07–0.2	0.2–0.3
	Total	σ_{α_u}	0.1–2	0.02–0.1	0.07–0.2	0.2–0.3

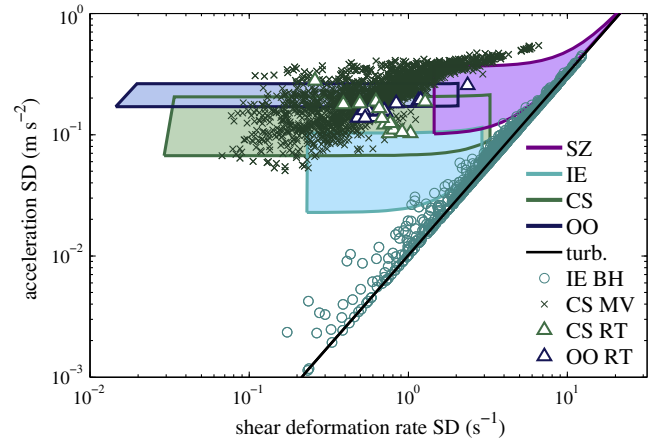


Fig. 9. Joint distributions of hydrodynamic signals, including typical ranges (color patches) and individual estimates (symbols) of co-occurring acceleration SD σ_{α_u} versus shear deformation rate SD $\sigma_{\Delta_{uz}}$ in each seascape. Colors indicate seascape: surf zone (SZ; magenta), inlets and estuaries (IE; cyan), continental shelf (CS; green), and open ocean (OO; blue). Symbols are observations from a tidal inlet (IE BH; cyan \circ) and the continental shelf (CS MV; green \times) and estimates from real-time buoy data on the continental shelf (CS RT; green Δ) and in the open ocean (CS RT; blue Δ). Solid black line is expected distribution for isotropic turbulence.

in different seascapes. The observed thresholds are instantaneous signals, whereas the typical signals are statistical representations. Although threshold signals have some non-zero probability of occurring in any seascape, this comparison identifies where above-threshold signals would occur frequently. The three species react to turbulence or shears with varying threshold values but would do so most frequently in coastal seascapes (Fig. 10). Dinoflagellates produce flashes of bioluminescence at shear stresses on the high end of typical signals in the surf zone (Fig. 10A), and spurious flashes would be rare in other seascapes; this rarity is precisely what makes bioluminescence startling to predators (Abrahams and Townsend, 1993). Oyster larvae swim faster or dive rapidly at high vorticities; these responses would occur most frequently in coastal seascapes, particularly in bottom boundary layers, but also could occur in the windiest near-surface conditions offshore (Fig. 10B). Larvae react similarly to high accelerations, but the threshold value exceeds typical accelerations outside the surf zone and may occur mainly in accelerating flows generated by suction-feeding fish (Higham et al., 2006; Holzman et al., 2008). Copepods perform escape jumps at deformation rates that vary with experimental conditions (Fig. 10C). Cultured copepods react to shears typical of all seascapes, whereas wild copepods react to higher shears typical only of the surf zone, and wild copepods in background turbulence react to still higher shears. Among these examples, the larger organisms reacted to weaker shears and could sense environmental fluid motions over a wider geographic range.

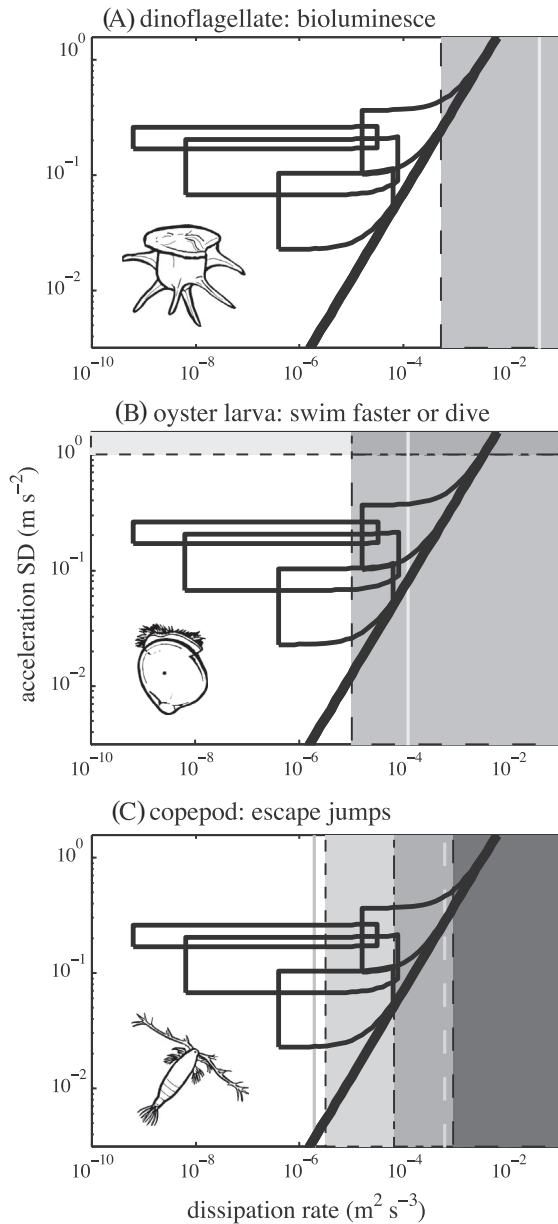


Fig. 10. Example behavior thresholds compared to hydrodynamic signals typical of seascapes. Spatial velocity gradients are expressed as dissipation rate. Black vertical or horizontal lines indicate threshold signals, and shaded regions span signal ranges where a reaction is expected. (A) Dinoflagellates (*Ceratocorys horrida*, $d = 70 \mu\text{m}$) bioluminesce above a threshold shear stress (dashed line, gray region; Latz et al., 2004). (B) Oyster larvae (*Crassostrea virginica*, $d = 310 \mu\text{m}$) swim faster upward or rapidly dive at above-threshold acceleration (dotted line, light gray) and vorticity (dashed line, medium gray) (Fuchs et al., 2013; Fuchs et al., 2015b; Fuchs et al., 2015a). (C) Adult copepods (*Acartia tonsa*, $d = 800\text{--}900 \mu\text{m}$) perform escape jumps at above-threshold longitudinal deformation rates in siphon flow. Estimated thresholds differ for cultured copepods (dotted line, light gray; Kjørboe et al., 1999), wild-caught copepods (dash-dotted line, medium gray; Gilbert and Buskey, 2005), and wild-caught copepods with background turbulence (dashed line, dark gray; Gilbert and Buskey, 2005). Black solid lines span ranges of typical dissipation rates and acceleration SD in each seascape as in Fig. 8B, and heavy black line indicates relationship between dissipation rates and acceleration SD in isotropic turbulence. Gray vertical lines indicate dissipation rate at which Kolmogorov length scale equals the body length d (solid, A–C) or a seta length (dashed, C; $\sim 200 \mu\text{m}$ Paffenhöfer, 1998).

To understand how the typical ranges of shears and accelerations relate to hydrodynamic sensing more generally, we also expressed these signals as the forces they would exert on plankters

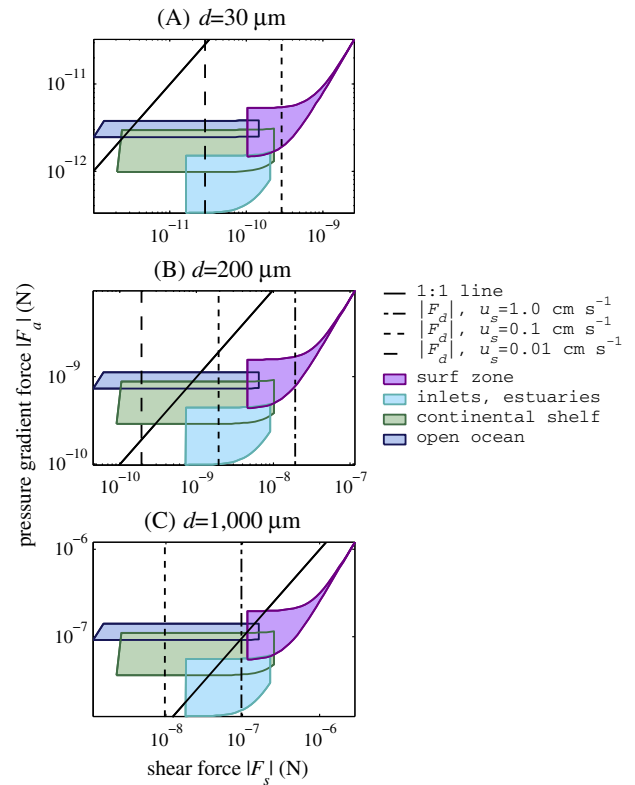


Fig. 11. Magnitudes of co-occurring shear force F_s (computed from shear using $\sigma_{\Delta u_z}$) and pressure gradient force F_a (computed from acceleration using σ_{a_z}) in each seascape as experienced by representative plankton: (A) dinoflagellates or small ciliates ($d = 30 \mu\text{m}$), (B) larger ciliates or small invertebrate larvae ($d = 200 \mu\text{m}$), and (C) larger larvae or small copepods ($d = 1000 \mu\text{m}$). Color patches are typical ranges of F_s and F_a in the surf zone (magenta), inlets and estuaries (cyan), continental shelf (green), and open ocean (blue). Solid line is 1:1. Drag force F_d likely represents a minimum detectable shear force and is shown for three swimming speeds: $u_s = 0.01 \text{ cm s}^{-1}$ (dashed line), $u_s = 0.1 \text{ cm s}^{-1}$ (dotted line), and $u_s = 1.0 \text{ cm s}^{-1}$ (dash-dotted line).

of different sizes. Shear forces F_s are calculated from shear deformation rate and would be dominated by turbulent motions, whereas pressure gradient forces F_a are calculated from fluid accelerations and are more dependent on wave motions (e.g., Fig. 9 axes). These estimates of F_s and F_a are standard deviations that describe the frequency distributions of forces rather than instantaneous values. Not unexpectedly, these forces varied among seascapes with a pattern similar to that of shear or dissipation rate and acceleration (Fig. 11). For a given plankter size, these forces spanned four and three orders of magnitude respectively, with the smallest shear forces in the open ocean, the smallest pressure gradient forces in inlets and estuaries, and the largest forces of both types in the surf zone. The shear force and pressure gradient force are proportional to powers of the radius, r^2 and r^3 respectively, so the absolute and relative magnitudes of F_s and F_a varied with plankton size. Smaller plankton generally would experience shear forces that were relatively larger than the pressure gradient forces, whereas larger plankton would experience these forces with more similar magnitudes. The drag force F_d depends on both size d and swimming speed u_s , and its relationship to F_s varied with the relative magnitudes of d and u_s . At slow to intermediate swimming speeds, plankton of each size category would experience shear forces greater than the drag force, suggesting that environmental shears would be detectable in surface waters of all seascapes.

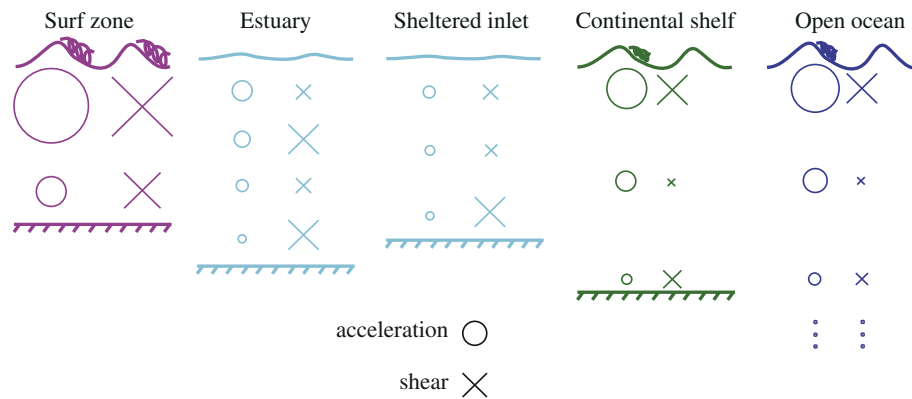


Fig. 12. Qualitative summary of spatial variation in the relative intensity of shears (or shear force) and accelerations (or pressure gradient forces). Symbols indicate shears (\times) or accelerations (\circ), size of symbol indicates relative magnitude, and colors indicate seascape: surf zone (magenta), inlets and estuaries (cyan), continental shelf (green), and open ocean (blue). Wavy lines indicate sea surface, hatched lines indicate seabed, and vertical dots indicate that water column continues downward. Depths are not to scale. (For interpretation of the references to color in this figure legend, the reader is referred to the web version of this article.)

5. Discussion

5.1. Seascape patterns in hydrodynamic signals

In surface waters, most seascapes are relatively indistinct from one another based on signals from turbulence alone but are hydrodynamically distinct based on combined signals from turbulence and waves. The largest dissipation rates are most often observed in shallow, nearshore waters, primarily due to wave breaking in surf zones and strong turbulence in the benthic boundary layers of inlets and estuaries (Figs. 3 and 4). Based on the ranges of frequently occurring ε , however, only the surf zone can be considered unique (Fig. 3). In offshore seascapes, the buoy estimates provide an important near-surface supplement to the published observations that often omit the upper 5–20 m. When the buoy estimates are included, there is substantial overlap in ranges of ε among other seascape types, and the maximum shears are similar among regions. Dissipation rates have similar maxima in all seascapes outside the surf zone, and the common idea that mixed-layer turbulence is weakest in the open ocean is primarily an artifact of previous under-sampling in the wave-affected surface layer. In contrast, enclosed and offshore seascapes are sharply delineated by wave-generated accelerations. When both turbulence and waves are accounted for, the distributions of shear and acceleration differ among ocean regions (Fig. 9). This spatial pattern demonstrates that it is possible for plankton to experience seascapes as distinct sensory environments (Fig. 12).

A combination of intense turbulence and large waves would make surf zones the most recognizable seascape. Surf-zone turbulence frequently generates shears of $1\text{--}100\text{ s}^{-1}$ (Fig. 3), while shoaling and breaking surface waves generate large accelerations. Observed cross-shore accelerations have standard deviations between 0.1 and 1 m s^{-2} (Elgar et al., 1988, 1990), and maximum instantaneous accelerations are larger ($\leq 10^2\text{ m s}^{-2}$; Gaylord, 1999; Elgar et al., 2001). This combination of strong signals distinguishes the surf zone from sheltered coastal habitats, where large shears can occur with small accelerations, and from the open ocean, where large accelerations can occur with small shears (Fig. 9). Surf zones are well studied in the context of hydrodynamic forces on benthic organisms (Denny et al., 1985; Helmuth and Denny, 2003), but effects of surf on plankton have received less attention. Our results support the concept that plankton could experience surf zones as hydrodynamically unique habitats (Gaylord et al., 2013).

Other sources of variability may make seascapes more hydrodynamically distinct than our analysis suggests. For example, inlets and estuaries often have asymmetric tides with stronger turbulence on flood and spring tides than on ebb and neap tides (Simpson et al., 1990; Geyer et al., 2000). These tidal variations were obscured by our use of a single mean $\log_{10}\varepsilon$ for each set of observations, and accounting for different tidal cycles likely would raise the estimated upper limits of frequently occurring ε in inlets and estuaries. Tidal currents also generate strong turbulence in bottom boundary layers (Figs. 4 and 9) with regularity. At the Barnstable Harbor inlet site, measured dissipation rates were $\varepsilon \geq 10^{-4}\text{ m}^2\text{ s}^{-3}$ half of the time, whereas offshore, such values occurred rarely. The BH data demonstrate that the bottom boundary layers in inlets can have strong turbulence and shears comparable to those in the surf zone while lacking any influence of waves (Fig. 9). With sufficiently resolved data it is possible that inlets and estuaries could be classified as the second-most turbulent seascape.

Within all seascape types, ranges of hydrodynamic signals will vary with stratification, seasonal cycles, and latitudinal gradients in wind and wave conditions. Stratification can cause dissipation rates and turbulent shears to vary by several orders of magnitude over a vertical scale of a few meters (Peters and Bokhorst, 2000; MacKinnon and Gregg, 2003; MacKinnon and Gregg, 2005a), although stratification has little effect on wave-induced accelerations. In estuaries where turbulence is driven primarily by tidal currents, salinity stratification can suppress turbulence in the surface and bottom boundary layers while aiding in the development of turbulence in shear layers (Stacey et al., 1999; Peters and Bokhorst, 2000; Stacey and Ralston, 2005; Scully et al., 2011). Stratification may differentiate flow regimes among otherwise similar habits such as inlets and estuaries (e.g., Fig. 12). Both temperature stratification and the intensity of wind-generated turbulence vary seasonally, with weaker stratification and stronger winds in winter months than in summer. Wind speed, wind variability, and significant wave height also generally increase with latitude and are highest at $\geq 40^\circ\text{N}$ or S (Caires and Sterl, 2005; Monahan, 2006). This synthesis includes data from a wide range of stratified conditions and buoy-based wave estimates from all seasons. There are few observations from high latitudes, however, and the buoy-based estimates of dissipation rate are only from late spring, omitting the windier winter months. Thus we likely underestimated the maximum, frequently occurring shears and accelerations in each seascape type (Figs. 8, 9), as well as the forces that these signals exert on plankton (Fig. 11).

Our analysis assumed that turbulence is isotropic, but stratification and fronts can generate shear layers where the dominant signals have a consistent orientation relative to gravity. In coastal regions, waves also become more anisotropic with depth, and vertical accelerations attenuate more rapidly than horizontal accelerations. Anisotropy is most relevant for plankters whose sensitivity to physical signals is directional, including copepods that use setae as external motion detectors (Fields, 2010) and mollusk larvae that use statocysts to sense changes in body orientation relative to gravity (Fuchs et al., 2015a). Although the anisotropy of waves is described by the wave equations (Table 1), the anisotropy of turbulence cannot be recaptured statistically from dissipation rates. Thus the estimates of typical shears may be less applicable to shear layers, which can occur in any seascape outside the surf zone. Shear layers can concentrate phytoplankton into thin layers through several mechanisms (Durham and Stocker, 2012) and concentrate zooplankton through feeding activity (e.g., Gallager et al., 2004; McManus et al., 2005; Menden-Deuer and Grünbaum, 2006). These biological hotspots may also be unique as sensory micro-environments, and more detailed observations are needed for comparing them to broader seascape regions.

Our analysis of seascapes is statistical, whereas individual plankters experience instantaneous signals that vary continuously in time. From the individual perspective, sensing depends on both the magnitude and duration of signals exceeding detection limits. The frequency of encounters with above-threshold signals depends on the process dominating the production of velocity gradients (Section 2.3). For example, wave-generated signals are normally distributed and could have magnitudes $\geq 3\sigma$ only $\sim 0.3\%$ of the time, whereas turbulence-generated signals have high kurtosis and could have magnitudes $\geq 3\sigma$ as much as 11% of the time (Chebyshev's inequality). The duration of strong signals depends on how plankton behave and interact with turbulent flow features, including coherent vortices and filaments. The time scales of plankter-flow interactions are a complex problem and have typically been addressed either using model plankters in realistic turbulence (Crimaldi et al., 2002; Koehl and Cooper, 2015; Pepper et al., 2015) or using real plankters in controlled vortices that mimic turbulent structures (Webster et al., 2015). There is no general theory relating hydrodynamic signals to interaction time scales, and our synthesis of typical signals provides a necessary baseline for quantifying the hydrodynamic signals experienced most frequently in different seascapes.

5.2. Implications for hydrodynamic sensing

Our results suggest that turbulence causes widespread interference in signaling among predators and prey. Many copepods and ciliates exhibit escape jumps when they encounter flows mimicking those produced by suction-feeding predators, with threshold shears of Δ_{ux} (or Δ_{uz}) $\approx 1\text{--}10\text{ s}^{-1}$ (Kiørboe et al., 1999; Jakobsen, 2001). These escape thresholds are often assumed to be higher than typical background levels (Kiørboe and Saiz, 1995; Kiørboe, 2013), but we found that offshore dissipation rates frequently exceed previously assumed limits, and background shears frequently exceed $\Delta_{uz} = 1\text{ s}^{-1}$ in all seascape types (Figs. 3 and 9). This background turbulence can dampen responses to predators or prey by reducing sensitivity and shortening the reaction distance at which plankton respond to fluid motions generated by other organisms (Costello et al., 1990; Saiz and Kiørboe, 1995; Visser, 2001). Reduced sensitivity or acclimation may help to limit spurious jumps; for example, the copepods *A. tonsa* perform escape jumps at threshold dissipation rates that are up to 100× higher in turbulence than in still water (Fig. 10C). At the lowest observed threshold, these copepods would waste considerable energy reacting to environmental fluid motions in their estuarine habitats,

whereas at the highest threshold, they could only escape predators that produce particularly strong signals. For species that acclimate, the threshold signal will increase with the frequency of strong signals, making it more difficult to generalize behaviors at sea from laboratory observations. The intensity of hydrodynamic noise will be high in all surface waters, and predator-prey signaling should be evaluated in this context.

Given this likelihood of strong signal interference, the ability to sense predators or prey may depend primarily on plankton depth distributions. Turbulence is often strongest in the surface and bottom boundary layers, which influence proportionally more of the water column in shallower nearshore habitats (Fig. 12). In inlets and estuaries, strong turbulence may make predator-prey signaling ineffective at any depth, whereas on the continental shelf and open ocean, predator-prey sensing will be most effective in deeper, calmer parts of the water column. Some plankton do avoid turbulent surface waters (e.g., Incze et al., 2001), but such behaviors usually are explained by the effects of turbulence on encounter rates, prey capture efficiency, and overall fitness (Rothschild and Osborn, 1988; Kiørboe and Saiz, 1995; Visser et al., 2009). It is unclear whether depth preferences also reflect hydrodynamic sensitivity or whether plankton have additional means of distinguishing among signals generated by animals and by physical processes.

This data synthesis also helps to place quantitative limits on the utility of turbulence intensity as an indicator of habitat type. It has been hypothesized that dispersing larvae of coastal species perceive strong turbulence as a signal of energetic nearshore waters and react by approaching the seabed to explore settlement sites (e.g., Chia et al., 1981; Fuchs et al., 2004). Here we found that typical dissipation rates approach $\varepsilon \approx 10^{-4}\text{ m}^2\text{ s}^{-3}$ (corresponding to $\Delta_{uz} \approx 4\text{ s}^{-1}$) in all seascapes but exceed this value only in surf zones (Figs. 3, 4). These high dissipation rates also occur regularly in the bottom boundary layers of inlets and estuaries (e.g., Fig. 6). Thus $\varepsilon \geq 10^{-4}\text{ m}^2\text{ s}^{-3}$ would be a decisive indicator of nearshore conditions. This hypothetical threshold exceeds the minimum dissipation rates that induce mollusk larvae to switch from upward swimming to sinking or diving in laboratory studies ($\varepsilon = 10^{-6}\text{--}10^{-5}\text{ m}^2\text{ s}^{-3}$; e.g., Fig. 10; Fuchs et al., 2004; Fuchs and DiBacco, 2011; Fuchs et al., 2013). However, larvae sink or dive more frequently at higher dissipation rates and thus would be more likely to react in energetic coastal zones. The threshold dissipation rates also occur more frequently in inlets and estuaries than offshore and would be indicative of enclosed habitats when they occur in the absence of large wave-generated accelerations found over the shelf and in the open ocean (Fig. 9).

Although hydrodynamic signals vary geographically, the ability of a plankter to discriminate among seascapes depends on how its sensory system detects fluid forces. All seascapes produce unique ranges of shear forces F_s and pressure gradient forces F_a (Fig. 11) and could be sensed as distinct environments by plankton that have some combination of receptors for these distinct forces. The shear force could be felt by external mechanosensors (e.g., cilia or antennae) as fluid deformation or by internal gravity detectors (e.g., statocysts or Müller's vesicles) as vorticity-induced rotation, whereas the pressure gradient force could be felt by accelerometers as a change in speed. A single sensor may be sufficient to identify the shallowest habitats: the surf zone could be detected as an above-threshold shear force by external mechanosensors or gravity detectors, whereas inlets and estuaries could be detected as a below-threshold (or absent) pressure gradient force by accelerometers. All habitats could be identified more decisively using multiple receptor types that detect both shear and pressure gradient forces. This potential capacity to identify specific habitats is most relevant for dispersing larval stages. Larvae of nearshore species may need only a

single receptor type to locate settlement sites, whereas larvae of offshore species may need multiple receptor types to definitively locate preferred habitats.

Sensitivity to shear forces could be limited by the drag on a plankter induced by its swimming motion (Fig. 11). Although the viscous drag force F_d depends on plankton behavior and the shear force F_s depends on fluid motions, both forces are generated by flow past the body that can physically deform the body wall or appendages. A plankter likely can only detect shear forces that exceed the drag force induced by its own swimming motion ($F_s > F_d$). While swimming, most plankters also generate fluid motions that raise the risk of being caught by a predator or of alerting prey items (Kjørboe, 2013), and these risks of moving may be exacerbated by a drag-induced loss of sensitivity to externally produced signals. There is evidence for this effect in zebrafish larvae, which detect predator-induced fluid motions with the lateral line and are less able to sense and avoid these motions while swimming (Feitl et al., 2010; Stewart et al., 2013). Swimming speed generally increases with body size (Hansen et al., 1997; Kjørboe and Jiang, 2012), and at typical swimming speeds the drag force falls squarely in the middle of typical shear forces produced by physical processes in most seascapes (Table 3; Fig. 11). Only stronger shears will be detectable, and thus the lower limits on detection may be set not just by receptor sensitivity, but also by swimming-induced drag acting as background noise.

Forces on sensors also vary with plankton size, and fluid motions will “feel” different to plankton of different sizes unless there is some compensation in receptor sensitivity. Compared to larger plankton, smaller plankton experience smaller hydrodynamic forces and may need more sensitive receptors to detect the same environmental signals (Fig. 11). Alternatively, smaller plankton could require a more intense hydrodynamic signal to sense fluid motion. There is evidence for this effect not just among our few example species (Fig. 10), but also within species whose sensing abilities have been tested over multiple size classes. For example, the copepods *A. tonsa* and *Temora longicornis* grow more sensitive to shears over the course of development; compared to copepodites or adults, the smaller nauplii escape at higher shear thresholds (Fields and Yen, 1997; Kjørboe et al., 1999; Titelman, 2001) and exhibit weaker behavioral responses to below-threshold shears (Woodson et al., 2005, 2007). Both among and within species, larger organisms should sense background turbulence over a relatively larger geographic range.

There are also geographic variations in how size affects the relative intensity of F_s and F_d . Under the most turbulent conditions in any seascape, a small ciliate would experience shear forces up to 100 times larger than the pressure gradient forces (Fig. 11A), while a larger copepod would experience shear forces and pressure gradient forces of similar magnitudes (Fig. 11C). In contrast, under calm conditions in the open ocean, the small ciliate would experience both forces with similar magnitudes, while the larger copepod would experience shear forces smaller than the pressure gradient forces. These comparisons suggest that a smaller, coastal organism would need more sensitive accelerometers or less sensitive mechanosensors to perceive the same relative signal balance as a larger, pelagic organism.

Although body size affects sensitivity to fluid forces, there is little evidence for any conditions where body size would make flow undetectable due to a mismatch in length scales of plankters and fluid motions. The three example species react to turbulence that has Kolmogorov scales much larger or smaller than the organisms themselves (Fig. 10). Copepods *A. tonsa* have varying sensitivity,

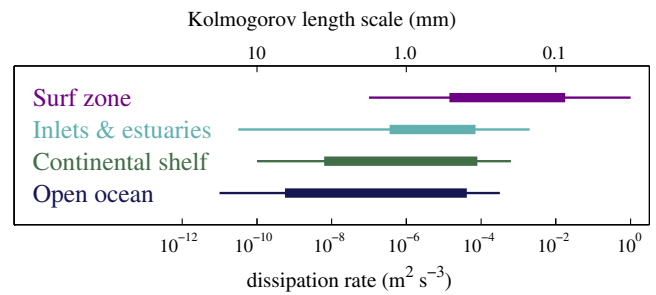


Fig. 13. Summary of dissipation rates (top x-axis) and associated Kolmogorov length scales (bottom x-axis; Eq. (3)). Horizontal lines span ranges of all estimates (thin lines) and log-space mean dissipation rates (thick lines) for each seascape (Fig. 3). Colors as in Fig. 3.

and depending on experimental conditions, they may react to turbulence with Kolmogorov scales ranging from larger than the body to smaller than the sensory setae (Fig. 10C). In practice, plankters potentially could sense any motions larger than their sensory organs. At sea the Kolmogorov scales are larger than most plankters' sensory organs. The exception is in the surf zone, where the smallest motions occur on scales of $\eta \sim 30 \mu\text{m}$ (Fig. 13) that may be imperceptible to some copepods with larger mechanosensory setae (up to $\sim 100 \mu\text{m}$ in length; Paffenhöfer, 1998). However, the smallest fluid motions occur in the most intense turbulence, where high-energy motions also occur on larger scales that would be sensible to virtually all organisms. The energy-containing scales of motion are nearly always larger than most planktonic organisms, and thus shear detection effectively depends only on signal magnitude.

Our results suggest that turbulence and waves together produce co-occurring shears and accelerations with rich information content, and multi-sensor systems could be powerful adaptations for survival. In calm environments with large Kolmogorov scales, plankters with different-sized shear sensors potentially could distinguish larger environmental fluid motions from smaller-scale motions produced by other plankton (Fields et al., 2002). Accelerations also potentially could be used to distinguish among seascapes or among signals generated by waves and organisms at different frequencies (Lang, 1980; Budelmann, 1989; Mooney et al., 2010). Dual sensor systems, e.g., a combination of external mechanosensors and internal gravity detectors or accelerometers, could be particularly useful to dispersing larvae that would benefit from an ability to sense broad-scale habitat differences. Plankton that sense multiple hydrodynamic signals may have a capacity to decode or differentiate signals produced by organisms and by physical processes in different seascapes.

Acknowledgments

Bob Chant, Judy Grassle, and anonymous reviewers provided helpful comments on the manuscript. Funding was provided by the National Science Foundation (OCE 1060622).

Appendix A. Data source tables

See Tables A.1 and A.2.

Table A.1

Sources used for dissipation rates in Fig. 3. N.D. indicates no depth data reported. Some depths were estimated from coordinates and NOAA bathymetry.

Location	Depth (m)	Dissipation rate ($\text{m}^2 \text{s}^{-3}$)	Reference
<i>1. Surf zones</i>			
Scripps Beach, La Jolla, CA	2.74	$10^{-7}-10^{-1}$	George et al. (1994)
Duck, NC	5	$10^{-6}-10^{-3.7}$	Trowbridge and Elgar (2001)
Cook's Beach, New Zealand	0.21	$10^{-5}-10^{-3}$	Bryan et al. (2003)
Tairua Beach, New Zealand	0.56	$10^{-4}-10^{-2.5}$	Bryan et al. (2003)
Duck, NC (0.56 mab)	3.2	$10^{-5.2}-10^{-3.9}$	Fedderson et al. (2007)
Duck, NC (1.32 mab)	3.2	$10^{-5.2}-10^{-3.9}$	Fedderson et al. (2007)
Duck, NC (1.86 mab)	3.2	$10^{-5}-10^{-3.8}$	Fedderson et al. (2007)
Hopkins Marine Station, CA (0.02 mab)	0.1	$10^{-3.5}-10^0$	Gaylord et al. (2013)
<i>2. Channels & estuaries</i>			
Stratford irrigation canal, WA	4.4	$10^{-6}-10^{-3.5}$	Gross and Nowell (1985)
Skagit Bay, WA (accelerating tide)	12	$10^{-5.4}-10^{-4.4}$	Gross and Nowell (1985)
Skagit Bay, WA (decelerating tide)	12	$10^{-5.4}-10^{-4.3}$	Gross and Nowell (1985)
Hudson River, NY	16	$10^{-8}-10^{-3}$	Peters (1997)
Cordova Channel, British Columbia	30	$10^{-7.8}-10^{-4.3}$	Lueck and Huang (1999)
Hudson estuary (neap tides)	15	$10^{-7}-10^{-4.2}$	Trowbridge et al. (1999)
Hudson estuary (spring tides)	15	$10^{-7.5}-10^{-3.8}$	Trowbridge et al. (1999)
Cordova Channel, British Columbia	30	$10^{-8}-10^{-4.9}$	Lu et al. (2000)
Cordova Channel, British Columbia	30	$10^{-8}-10^{-4.3}$	Lu et al. (2000)
Hudson River estuary, NY (neap tides)	13	$10^{-7}-10^{-4.8}$	Peters and Bokhorst (2000)
Hudson River estuary, NY (spring tides)	13	$10^{-5.9}-10^{-4.2}$	Peters and Bokhorst (2000)
Pickering Passage, WA	22.5	$10^{-8}-10^{-4}$	Lien and Sanford (2004)
San Francisco Bay, CA	2.5	$10^{-7.2}-10^{-3}$	Jones and Monismith (2008)
Barnstable Harbor, MA	6.8	$10^{-10.5}-10^{-3}$	Fuchs et al. (2010)
Merrimack River (unstratified)	7	$10^{-5.1}-10^{-3.2}$	Scully et al. (2011)
Merrimack River (stratified)	7	$10^{-5.7}-10^{-3.6}$	Scully et al. (2011)
Puget Sound (Nodule Point)	22	$10^{-7}-10^{-4.2}$	Thomson et al. (2012)
Puget Sound (Admiralty Head)	62	$10^{-6.5}-10^{-2.7}$	Thomson et al. (2012)
<i>3. Continental shelves</i>			
Emerald Basin, Scotian shelf (upper mixed layer)	195	$10^{-7.5}-10^{-5.5}$	Oakey and Elliott (1982)
Emerald Basin, Scotian shelf (lower mixed layer)	195	$10^{-9}-10^{-6}$	Oakey and Elliott (1982)
Shelf near Vancouver I.	135	$10^{-9.5}-10^{-6}$	Dewey and Crawford (1988)
Hecate Strait	35	$10^{-6.3}-10^{-5.2}$	Dewey and Crawford (1988)
Scotian shelf	105	$10^{-10}-10^{-6}$	Sandstrom and Oakey (1995)
Maryland coast	89	$10^{-4.8}-10^{-3.4}$	Drennan et al. (1996)
Irish Sea	60	$10^{-6.5}-10^{-4}$	Simpson et al. (1996)
Irish Sea	90	$10^{-7}-10^{-4.5}$	Simpson et al. (1996)
Irish Sea	90	$10^{-8}-10^{-6}$	Simpson et al. (1996)
Satellite Channel near Vancouver I.	80	$10^{-9.5}-10^{-6}$	Lueck et al. (1997)
New York Bight (0.1–1.4 mab)	15	$10^{-5.5}-10^{-5.0}$	Doron et al. (2001)
Emerald Bank, Scotian Shelf	100	$10^{-10}-10^{-5}$	Greenan et al. (2001)
New England shelf near Martha's Vineyard (4.35 mab)	70	$10^{-9}-10^{-5.5}$	Shaw et al. (2001)
New England shelf near Martha's Vineyard (1.65 mab)	70	$10^{-8}-10^{-5}$	Shaw et al. (2001)
New England shelf near Martha's Vineyard (0.74 mab)	70	$10^{-7.5}-10^{-4.8}$	Shaw et al. (2001)
Oregon shelf	120	$10^{-8}-10^{-5.5}$	Klymak and Moum (2003)
Columbia River mouth, OR	109	$10^{-9}-10^{-5}$	Moum et al. (2003)
Red Wharf Bay, Irish Sea	28	$10^{-8}-10^{-4.1}$	Rippeth et al. (2003)
near I. of Mull (1.93 mbs)	40–110	$10^{-7.3}-10^{-4.1}$	Thorpe et al. (2003)
near I. of Mull (10.4 mbs)	40–110	$10^{-7.3}-10^{-4.9}$	Thorpe et al. (2003)
New England Shelf	70	$10^{-10}-10^{-6}$	MacKinnon and Gregg (2005b)
South of Martha's Vineyard	16	$10^{-7.2}-10^{-3.2}$	Gerbi et al. (2009)
Monterey Bay	85	$10^{-7}-10^{-5.3}$	Gregg and Horne (2009)
Saanitch Inlet	240	$10^{-8.9}-10^{-7.9}$	Rousseau et al. (2010)
Florida Current	15	$10^{-8}-10^{-4}$	Davis and Monismith (2011)
<i>4. Open ocean</i>			
Sargasso Sea	5330	$10^{-9.6}-10^{-5.5}$	Gargett et al. (1979)
Ocean station P (light winds)	4220	$10^{-11}-10^{-7.5}$	Dillon and Caldwell (1980)
Ocean station P (strong winds)	4220	$10^{-8}-10^{-6.5}$	Dillon and Caldwell (1980)
Equatorial Atlantic	N.D.	$10^{-9.5}-10^{-5.5}$	Osborn and Bilodeau (1980)
Equatorial Pacific (< 0.5° from equator)	4800	$10^{-9}-10^{-7}$	Crawford (1982)
Equatorial Pacific (> 1° from equator)	4800	$10^{-9.8}-10^{-7.4}$	Crawford (1982)
Rockall Trough	N.D.	$10^{-8.2}-10^{-6.3}$	Oakey (1982)
California Current	5000	$10^{-9.5}-10^{-8.1}$	Gregg et al. (1986)

(continued on next page)

Table A.1 (continued)

Location	Depth (m)	Dissipation rate ($\text{m}^2 \text{s}^{-3}$)	Reference
Equatorial Pacific	4000	$10^{-10.5} - 10^{-7}$	Moum et al. (1986)
NW Pacific	N.D.	$10^{-8.7} - 10^{-4.5}$	Osborn et al. (1992)
offshore of Oregon	1000–2000	$10^{-8.7} - 10^{-4}$	Anis and Moum (1995)
Equatorial Pacific (50 mbs)	3800	$10^{-10} - 10^{-5}$	Moum et al. (1995)
Equatorial Pacific (75 mbs)	3800	$10^{-10} - 10^{-5.2}$	Moum et al. (1995)
Equatorial Pacific (100 mbs)	3800	$10^{-10} - 10^{-6.5}$	Moum et al. (1995)
Equatorial Pacific (125 mbs)	3800	$10^{-10} - 10^{-6.5}$	Moum et al. (1995)
W. Equatorial Pacific	4000	$10^{-7} - 10^{-3.5}$	Soloviev and Lukas (2003)
Equatorial Pacific	3800	$10^{-9} - 10^{-5}$	Moum et al. (2009)
Ocean Station P	4220	$10^{-10} - 10^{-7.3}$	Rousseau et al. (2010)

Table A.2

National Data Buoy Center buoys used for analysis. Buoy type abbreviations: DS, discus buoy; WR, waverider buoys; MB, moored buoys; ST, C-MAN station. Only discus buoys record complete real-time data used for estimating dissipation rates (Fig. 3); all buoys record historical data used in calculating wave-generated signal variances (Fig. 5).

Buoy #	Type	Name	Ocean	Depth (m)	Seascape
41002	DS	S Hatteras	Atlantic	4297	Open ocean
41004	DS	Edisto, near Charleston SC	Atlantic	38.4	Continental shelf
41008	DS	Grays Reef GA	Atlantic	19.5	Continental shelf
41009	DS	Canaveral FL	Atlantic	40.5	Continental shelf
41040	DS	N Equatorial One	Atlantic	4900	Open ocean
41041	DS	N Equatorial Two	Atlantic	3485	Open ocean
41043	DS	NE Puerto Rico	Atlantic	5292	Open ocean
41044	DS	NE St. Martin	Atlantic	4536	Open ocean
41046	DS	E Bahamas	Atlantic	5515	Open ocean
41047	DS	NE Bahamas	Atlantic	5315	Open ocean
41048	DS	W Bermuda	Atlantic	5340	Open ocean
41109	WR	New River Inlet NC	Atlantic	13.2	Continental shelf
41110	WR	Masonboro Inlet NC	Atlantic	15.7	Continental shelf
41113	WR	Cape Canaveral Nearshore FL	Atlantic	9.87	Continental shelf
42012	DS	Orange Beach AL	Atlantic	27.7	Continental shelf
42036	DS	W Tampa FL	Atlantic	50.6	Continental shelf
44005	DS	Gulf of Maine	Atlantic	206	Continental shelf
44017	DS	Montauk Pt. NY	Atlantic	52.4	Continental shelf
44020	DS	Nantucket Sound	Atlantic	11	Continental shelf
44027	DS	Jonesport ME	Atlantic	178.6	Continental shelf
44056	WR	Duck NC	Atlantic	17.4	Continental shelf
44066	DS	Texas Tower NJ #4	Atlantic	78	Continental shelf
44095	WR	Oregon Inlet NC	Atlantic	18.3	Continental shelf
44098	WR	Jeffrey's Ledge NH	Atlantic	76.5	Continental shelf
46002	DS	W Oregon	Pacific	3368	Open ocean
46014	DS	Pt. Arena CA	Pacific	256	Continental shelf
46026	DS	San Francisco CA	Pacific	53	Continental shelf
46027	DS	St. Georges CA	Pacific	46	Continental shelf
46050	DS	Stonewall Bank OR	Pacific	137.2	Continental shelf
46066	DS	S Kodiak	Pacific	4545	Open ocean
46211	WR	Grays Harbor WA	Pacific	38.5	Continental shelf
46215	WR	Diablo Canyon CA	Pacific	22.86	Continental shelf
46217	WR	Anacapa Passage CA	Pacific	114	Continental shelf
46221	WR	Santa Monica Bay CA	Pacific	363	Continental shelf
46229	WR	Umpqua Offshore OR	Pacific	182.9	Continental shelf
46240	WR	Cabrillo Point CA	Pacific	18.5	Continental shelf
46246	WR	Ocean Station PAPA	Pacific	4252	Open ocean
51000	DS	N Hawaii one	Pacific	4845	Open ocean
51100	DS	N Hawaii two	Pacific	4754.9	Open ocean
LJPC1	ST	La Jolla CA	Pacific	7.51	Continental shelf

References

- Abrahams, M.V., Townsend, L.D., 1993. Bioluminescence in dinoflagellates: a test of the burglar alarm hypothesis. *Ecology* 74, 258–260.
- Agrawal, Y.C., Terray, E.A., Donelan, M.A., Hwang, P.A., Williams III, A.J., Drennan, W. M., Kahma, K.K., Kitaigorodskii, S.A., 1992. Enhanced dissipation of kinetic energy beneath surface waves. *Nature* 359, 219–220.
- Anis, A., Moum, J.N., 1995. Surface wave–turbulence interactions: scaling $\varepsilon(z)$ near the sea surface. *Journal of Physical Oceanography* 25, 2025–2045.
- Barile, P.J., Stoner, A.W., Young, C.M., 1994. Phototaxis and vertical migration of the queen conch (*Strombus gigas* Linne) veliger larvae. *Journal of Experimental Marine Biology and Ecology* 183, 147–162.
- Batchelor, G.K., 1953. *The Theory of Homogeneous Turbulence*. Cambridge University Press, London.
- Beck, C., 2003. Lagrangian acceleration statistics in turbulent flows. *Europhysics Letters* 64, 151–157.
- Bryan, K.R., Black, K.P., Gorman, R.M., 2003. Spectral estimates of dissipation rate within and near the surf zone. *Journal of Physical Oceanography* 33, 979–993.
- Budelmann, B.-U., 1988. Morphological diversity of equilibrium receptor systems in aquatic invertebrates. In: Atema, J., Fay, R.R., Popper, A.N., Tavolga, W.N. (Eds.), *Sensory Biology of Aquatic Animals*. Springer-Verlag, New York, pp. 757–782.
- Budelmann, B.-U., 1989. Hydrodynamic receptor systems in invertebrates. In: Coombs, S., Görnerand, P., Münz, H. (Eds.), *The Mechanosensory Lateral Line*. Springer-Verlag, New York, pp. 607–631.

- Burdick, D.S., Hartline, D.K., Lenz, P.H., 2007. Escape strategies in co-occurring calanoid copepods. *Limnology and Oceanography* 52, 2373–2385.
- Buskey, E.J., Lenz, P.H., Hartline, D.K., 2012. Sensory perception, neurobiology, and behavioral adaptations for predator avoidance in planktonic copepods. *Animal Behaviour* 20, 57–66.
- Caires, S., Sterl, A., 2005. 100-year return value estimates for ocean wind speed and significant wave height from the ERA-40 data. *Journal of Climate* 19, 1032–1048.
- Chia, F.S., Koss, R., Bickell, L.R., 1981. Fine structural study of the statocysts in the veliger larva of the nudibranch, *Rostanga pulchra*. *Cell and Tissue Research* 214, 67–80.
- Churchill, J.H., Plueddemann, A.J., Faluotico, S.M., 2006. Extracting Wind Sea and Swell from Directional Wave Spectra Derived from a Bottom-Mounted ADCP. Woods Hole Oceanographic Institution Tech. Rep. WHOI-2006-13, 34 pp.
- Clift, R., Grace, J.R., Weber, M.E., 1978. Bubbles, Drops, and Particles. Academic Press, New York.
- Costello, J.H., Strickler, J.R., Marrasé, C., Trager, G., Zeller, R., Freise, A.J., 1990. Grazing in a turbulent environment: behavioral response of a calanoid copepod, *Centropages hamatus*. *Proceedings of the National Academy of Sciences* 87, 1648–1652.
- Craig, P.D., Banner, M.L., 1994. Modeling wave-enhanced turbulence in the ocean surface layer. *Journal of Physical Oceanography* 24, 2546–2559.
- Crawford, W.R., 1982. Pacific equatorial turbulence. *Journal of Physical Oceanography* 12, 1137–1149.
- Crimaldi, J.P., Thompson, J.K., Rosman, J.H., Lowe, R.J., Koseff, J.R., 2002. Hydrodynamics of larval settlement: the influence of turbulent stress events at potential recruitment sites. *Limnology and Oceanography* 47, 1137–1151.
- Davis, K.A., Monismith, S.G., 2011. The modification of bottom boundary layer turbulence and mixing by internal waves shoaling on a barrier reef. *Journal of Physical Oceanography* 41, 2223–2241.
- Denny, M.W., Daniel, T.L., Koehl, M.A.R., 1985. Mechanical limits to size in wave-swept organisms. *Ecological Monographs* 55, 69–102.
- Dewey, R.K., Crawford, W.R., 1988. Bottom stress estimates from vertical dissipation rate profiles on the continental shelf. *Journal of Atmospheric and Oceanic Technology* 18, 1167–1177.
- Dillon, T.M., Caldwell, D.R., 1980. The Batchelor spectrum and dissipation in the upper ocean. *Journal of Geophysical Research* 85, 1910–1916.
- Doron, P., Bertuccioli, L., Katz, J., Osborn, T.R., 2001. Turbulence characteristics and dissipation estimates in the coastal ocean bottom boundary layer from PIV data. *Journal of Physical Oceanography* 31, 2108–2134.
- Drennan, W.M., Donelan, M.A., Terray, E.A., Katsaros, K.B., 1996. Oceanic turbulence dissipation measurements in SWADE. *Journal of Physical Oceanography* 26, 808–815.
- Durham, W.M., Stocker, R., 2012. Thin phytoplankton layers: characteristics, mechanisms, and consequences. *Annual Review of Marine Science* 4, 177–207.
- Echevarria, M.L., Wolfe, G.V., Strom, S.L., Taylor, A.R., 2014. Connecting alveolate cell biology with trophic ecology in the marine plankton using the ciliate *Favella* as a model. *FEMS Microbiology Ecology* 90, 18–38.
- Elgar, S., Freilich, M.H., Guza, R.T., 1990. Model-data comparisons of moments of nonbreaking shoaling surface gravity waves. *Journal of Geophysical Research* 95, 16,055–16,063.
- Elgar, S., Gallagher, E.L., Guza, R.T., 2001. Nearshore sandbar migration. *Journal of Geophysical Research* 106, 11,623–11,627.
- Elgar, S., Guza, R.T., Freilich, M.H., 1988. Eulerian measurements of horizontal accelerations in shoaling gravity waves. *Journal of Geophysical Research* 93, 9261–9269.
- Esaias, W.E., Curl Jr., H.C., 1972. Effect of dinoflagellate bioluminescence on copepod ingestion rates. *Limnology and Oceanography* 17, 901–906.
- Fedderson, F., Trowbridge, J.H., Williams III, A.J., 2007. Vertical structure of dissipation in the nearshore. *Journal of Physical Oceanography* 37, 1764–1777.
- Feigenbaum, D., Reeve, M.R., 1977. Prey detection in the Chaetognatha: response to a vibrating probe and experimental determination of attack distance in large aquaria. *Limnology and Oceanography* 22, 1052–1058.
- Feitl, K.E., Ngo, V., McHenry, M.J., 2010. Are fish less responsive to a flow stimulus when swimming? *Journal of Experimental Biology* 213, 3131–3137.
- Fields, D.M., 2010. Orientation affects the sensitivity of *Acartia tonsa* to fluid mechanical signals. *Marine Biology* 157, 505–514.
- Fields, D.M., Shaeffer, D.S., Weissburg, M.J., 2002. Mechanical and neural responses from the mechanosensory hairs on the antennule of *Gaussia princeps*. *Marine Ecology: Progress Series* 227, 173–186.
- Fields, D.M., Yen, J., 1997. The escape behavior of marine copepods in response to a quantifiable fluid mechanical disturbance. *Journal of Plankton Research* 19, 1289–1304.
- Fraser, P.J., 2006. Review: depth, navigation and orientation in crabs: angular acceleration, gravity and hydrostatic pressure sensing during path integration. *Marine and Freshwater Behaviour and Physiology* 39, 87–97.
- Fuchs, H.L., Christman, A.J., Gerbi, G.P., Hunter, E.J., Diez, F.J., 2015a. Directional flow sensing by passively stable larvae. *Journal of Experimental Biology* 218, 2782–2792.
- Fuchs, H.L., DiBacco, C., 2011. Mussel larval responses to turbulence are unaltered by larval age or light conditions. *Limnology and Oceanography: Fluids Environments* 1, 120–134.
- Fuchs, H.L., Gerbi, G.P., Hunter, E.J., Christman, A.J., Diez, F.J., 2015b. Hydrodynamic sensing and behavior by oyster larvae in turbulence and waves. *Journal of Experimental Biology* 218, 1419–1432.
- Fuchs, H.L., Hunter, E.J., Schmitt, E.L., Guazzo, R.A., 2013. Active downward propulsion by oyster larvae in turbulence. *Journal of Experimental Biology* 216, 1458–1469.
- Fuchs, H.L., Mullineaux, L.S., Solow, A.R., 2004. Sinking behavior of gastropod larvae (*Ilyanassa obsoleta*) in turbulence. *Limnology and Oceanography* 49, 1937–1948.
- Fuchs, H.L., Neubert, M.G., Mullineaux, L.S., 2007. Effects of turbulence-mediated larval behavior on larval supply and settlement in tidal currents. *Limnology and Oceanography* 52, 1156–1165.
- Fuchs, H.L., Reidenbach, M.A., 2013. Biophysical constraints on optimal patch lengths for settlement of a reef-building bivalve. *PLoS ONE* 8, e71506. <http://dx.doi.org/10.1371/journal.pone.0071506>.
- Fuchs, H.L., Solow, A.R., Mullineaux, L.S., 2010. Larval responses to turbulence and temperature in a tidal inlet: Habitat selection by dispersing gastropods? *Journal of Marine Research* 68, 153–188.
- Fujimura, A.G., Reniers, A.J.H.M., Paris, C.B., Shanks, A.L., MacMahan, J.H., Morgan, S.G., 2014. Numerical simulations of larval transport into a rip-channeled surf zone. *Limnology and Oceanography* 59, 1434–1447.
- Gallager, S.M., Yamazaki, H., Davis, C.S., 2004. Contribution of fine-scale vertical structure and swimming behavior to formation of plankton layers on Georges Bank. *Marine Ecology: Progress Series* 267, 27–43.
- Gallin, E.K., Wiederhold, M.L., 1977. Response of *Aplysia* statocyst receptor cells to physiological stimulation. *Journal of Physiology* 266, 123–137.
- Gargett, A., Wells, J., Tejada-Martínez, A.E., Grosch, C.E., 2004. Langmuir supercells: a mechanism for sediment resuspension and transport in shallow seas. *Science* 306, 1925–1928.
- Gargett, A.E., Sanford, T.B., Osborn, T.R., 1979. Surface mixing layers in the Sargasso Sea. *Journal of Physical Oceanography* 9, 1090–1111.
- Gaylord, B., 1999. Detailing agents of physical disturbance: wave-induced velocities and accelerations on a rocky shore. *Journal of Experimental Marine Biology and Ecology* 239, 85–124.
- Gaylord, B., Hodin, J., Ferner, M.C., 2013. Turbulent shear spurs settlement in larval sea urchins. *Proceedings of the National Academy of Sciences* 110, 6901–6906.
- Gemmrich, J., 2010. Strong turbulence in the wave crest region. *Journal of Physical Oceanography* 40, 583–595.
- Gemmrich, J.R., Farmer, D.M., 2004. Near-surface turbulence in the presence of breaking waves. *Journal of Physical Oceanography* 34, 1067–1086.
- Gemmrich, J.R., Mudge, T.D., Polonichko, V.D., 1994. On the energy input from wind to surface waves. *Journal of Physical Oceanography* 24, 2413–2417.
- George, R., Flick, R.E., Guza, R.T., 1994. Observations of turbulence in the surf zone. *Journal of Geophysical Research* 99, 801–810.
- Gerbi, G.P., Trowbridge, J.H., Terray, E.A., Plueddemann, A.J., Kukulka, T., 2009. Observations of turbulence in the ocean surface boundary layer: energetics and transport. *Journal of Physical Oceanography* 39, 1077–1096.
- Geyer, W.R., Scully, M.E., Ralston, D.K., 2008. Quantifying vertical mixing in estuaries. *Environmental Fluid Mechanics* 8, 495–509.
- Geyer, W.R., Trowbridge, J.H., Bowen, M.M., 2000. The dynamics of a partially mixed estuary. *Journal of Physical Oceanography* 30, 2035–2048.
- Gilbert, O.M., Buskey, E.J., 2005. Turbulence decreases the hydrodynamic predator sensing ability of the calanoid copepod *Acartia tonsa*. *Journal of Plankton Research* 27, 1067–1071.
- Gill, C.W., Crisp, D.J., 1985. Sensitivity of intact and antennule amputated copepods to water disturbance. *Marine Ecology: Progress Series* 21, 221–227.
- Gillespie, P.G., Walker, R.G., 2001. Molecular basis of mechanosensory transduction. *Nature* 413, 194–202.
- Gotoh, T., Fukayama, D., Nakano, T., 2002. Velocity field statistics in homogeneous steady turbulence obtained using a high-resolution direct numerical simulation. *Physics of Fluids* 14, 1065–1081.
- Grant, W.D., Madsen, O.S., 1986. The continental-shelf bottom boundary layer. *Annual Review of Fluid Mechanics* 18, 265–305.
- Greenan, B.J.W., Oakey, N.S., Dobson, F.W., 2001. Estimates of dissipation in the ocean mixed layer using a quasi-horizontal microstructure profiler. *Journal of Physical Oceanography* 31, 992–1004.
- Greene, C.H., Landry, M.R., Monger, B.C., 1986. Foraging behavior and prey selection by the ambush entangling predator *Pleurobrachia bachei*. *Ecology* 67, 1493–1501.
- Gregg, M.C., D'Asaro, E.A., Shay, T.J., Larson, N., 1986. Observations of persistent mixing and near-inertial internal waves. *Journal of Physical Oceanography* 16, 856–885.
- Gregg, M.C., Horne, J.K., 2009. Turbulence, acoustic backscatter, and pelagic nekton in Monterey Bay. *Journal of Physical Oceanography* 39, 1097–1114.
- Gross, T.F., Nowell, A.R.M., 1985. Spectral scaling in a tidal boundary layer. *Journal of Physical Oceanography* 15, 496–508.
- Grünbaum, D., Strathmann, R.R., 2003. Form, performance and trade-offs in swimming and stability of armed larvae. *Journal of Marine Research* 61, 659–691.
- Guasto, J.S., Rusconi, R., Stocker, R., 2012. Fluid mechanics of planktonic microorganisms. *Annual Review of Fluid Mechanics* 44, 373–400.
- Haddock, S.H.D., Moline, M.A., Case, J.F., 2010. Bioluminescence in the sea. *Annual Review of Marine Science* 2, 443–493.
- Hansen, B., 1991. Feeding behaviour in larvae of the opisthobranch *Philine aperta*. II. Food size spectra and particle selectivity in relation to larval behaviour and morphology of the velar structures. *Marine Biology* 111, 263–270.
- Hansen, P.J., Bjørnsen, P.K., Hansen, B.W., 1997. Zooplankton grazing and growth: scaling within the 2–2000- μm body size range. *Limnology and Oceanography* 42, 687–704.
- Hasselmann, K., Barnett, T.P., Bouws, E., Carlson, H., Cartwright, D.E., Enke, K., Ewing, J.A., Gienapp, H., Hasselmann, D.E., Kruseman, P., Meerburg, A., Müller, P.,

- Olbers, Richter, K., Sell, W., Walden, H., 1973. Measurements of wind-wave growth and swell decay during the Joint North Sea Wave Project (JONSWAP). *Deutsche Hydrographische Zeitschrift A8* (Suppl.), 1–95.
- Helmuth, B., Denny, M.W., 2003. Predicting wave exposure in the rocky intertidal zone: do bigger waves always lead to larger forces? *Limnology and Oceanography* 48, 1338–1345.
- Heuch, P.A., Karlsen, H.E., 1997. Detection of infrasonic water oscillations by copepodids of *Lepeophtheirus salmonis* (Copepoda: Caligida). *Journal of Plankton Research* 19, 735–747.
- Higham, T.E., Day, S.W., Wainwright, P.C., 2006. Multidimensional analysis of suction feeding performance in fishes: fluid speed, acceleration, strike accuracy and the ingested volume of water. *Journal of Experimental Biology* 209, 2713–2725.
- Holthuijsen, L.H., 2007. *Waves in Oceanic and Coastal Waters*. University Press, Cambridge, UK.
- Holzman, R., Collar, D.C., Day, S.W., Bishop, K.L., Wainwright, P.C., 2008. Scaling of suction-induced flows in bluegill: morphological and kinematic predictors for the ontogeny of feeding performance. *Journal of Experimental Biology* 211, 2658–2668.
- Hwang, P.A., 2009. Estimating the effective energy transfer velocity at air–sea interface. *Journal of Geophysical Research* 114, C11011.
- Incze, L.S., Hebert, D., Wolff, N., Oakey, N., Dye, D., 2001. Changes in copepod distributions associated with increased turbulence from wind stress. *Marine Ecological: Progress Series* 213, 229–240.
- Jackson, N.L., 1995. Wind and waves: influence of local and non-local waves on mesoscale beach behavior in estuarine environments. *Annals of the Association of American Geographers* 85, 21–37.
- Jackson, N.L., Nordstrom, K.F., 1992. Site specific controls on wind and wave processes and beach mobility on estuarine beaches in New Jersey, USA. *Journal of Coastal Research* 8, 88–98.
- Jackson, N.L., Nordstrom, K.F., 1994. The mobility of beach fill in front of a seawall on an estuarine shoreline, Cliffwood Beach, New Jersey, USA. *Ocean & Coastal Management* 23, 149–166.
- Jackson, N.L., Nordstrom, K.F., Eliot, I., Masselink, G., 2002. ‘Low energy’ sandy beaches in marine and estuarine environments: a review. *Geomorphology* 48, 147–162.
- Jakobsen, H.H., 2001. Escape response of planktonic protists to fluid mechanical signals. *Marine Ecological: Progress Series* 214, 67–78.
- Jakobsen, H.H., 2002. Escape of protists in predator-generated feeding currents. *Aquatic Microbial Ecology* 26, 271–281.
- Jones, N.L., Monismith, S.G., 2008. The influence of whitecapping waves on the vertical structure of turbulence in a shallow estuarine embayment. *Journal of Physical Oceanography* 38, 1563–1580.
- Jonsson, P.R., André, C., Lindegarth, M., 1991. Swimming behaviour of marine bivalve larvae in a flume boundary-layer flow: evidence for near-bottom confinement. *Marine Ecological: Progress Series* 79, 67–76.
- Jumars, P.A., Trowbridge, J.H., Boss, E., Karp-Boss, L., 2009. Turbulence–plankton interactions: a new cartoon. *Marine Ecology* 30, 133–150.
- Kamykowski, D., McCollum, S.A., 1986. The temperature acclimatized swimming speed of selected marine dinoflagellates. *Journal of Plankton Research* 8, 275–287.
- Kamykowski, D., Reed, R.E., Kirkpatrick, G.J., 1992. Comparison of sinking velocity, swimming velocity, rotation and path characteristics among six marine dinoflagellate species. *Marine Biology* 113, 319–328.
- Karp-Boss, L., Jumars, P.A., 1998. Motion of diatom chains in steady shear flow. *Limnology and Oceanography* 43, 1767–1773.
- Kessler, J.O., 1986. The external dynamics of swimming micro-organisms. *Progress in Psychological Research* 4, 257–291.
- Kingsford, M.J., Leis, J.M., Shanks, A., Lindeman, K.C., Morgan, S.G., Pineda, J., 2002. Sensory environments, larval abilities and local self-recruitment. *Bulletin of Marine Science* 70 (Suppl.), 309–340.
- Kjørboe, T., 2011. How zooplankton feed: mechanisms, traits and trade-offs. *Biological Reviews* 86, 311–339.
- Kjørboe, T., 2013. Attack or attacked: the sensory and fluid mechanical constraints of copepods’ predator–prey interactions. *Integrative and Comparative Biology* 53, 821–831.
- Kjørboe, T., Jang, H., 2012. To eat and not be eaten: optimal foraging behaviour in suspension feeding copepods. *Journal of Royal Society Interface*, 20120693. <http://dx.doi.org/10.1098/rsif.2012.0693>.
- Kjørboe, T., Saiz, E., 1995. Planktivorous feeding in calm and turbulent environments, with emphasis on copepods. *Marine Ecological: Progress Series* 122, 135–145.
- Kjørboe, T., Saiz, E., Visser, A., 1999. Hydrodynamic signal perception in the copepod *Acartia tonsa*. *Marine Ecological: Progress Series* 179, 97–111.
- Klymak, J.M., Moum, J.N., 2003. Internal solitary waves of elevation advancing on a shoaling shelf. *Geophysical Research Letters* 30, 2045. <http://dx.doi.org/10.1029/2003GL017706>.
- Koehl, M.A.R., Cooper, T., 2015. Swimming in an unsteady world. *Integrative and Comparative Biology* 55, 683–697.
- Koehl, M.A.R., Crimaldi, J.P., Dombroski, D.E., 2013. Wind chop and ship wakes determine hydrodynamic stresses on larvae settling on different microhabitats in fouling communities. *Marine Ecological: Progress Series* 479, 47–62.
- Kolmogorov, A.N., 1962. A refinement of previous hypotheses concerning the local structure of turbulence in a viscous incompressible fluid at high Reynolds number. *Journal of Fluid Mechanics* 13, 82–85.
- Kurose, R., Komori, S., 1999. Drag and lift forces on a rotating sphere in a linear shear flow. *Journal of Fluid Mechanics* 384, 183–206.
- Lang, H.H., 1980. Surface wave discrimination between prey and nonprey by the back swimmer *Notonecta glauca* L. (Hemiptera, Heteroptera). *Behavioral Ecology and Sociobiology* 6, 233–246.
- Latz, M.I., Case, J.F., Gran, R.L., 1994. Excitation of bioluminescence by laminar fluid shear associated with simple Couette flow. *Limnology and Oceanography* 39, 1424–1439.
- Latz, M.I., Nauen, J.C., Rohr, J., 2004. Bioluminescence response of four species of dinoflagellates to fully developed pipe flow. *Journal of Plankton Research* 26, 1529–1546.
- Latz, M.I., Rohr, J., 1999. Luminescent response of the red tide dinoflagellate *Lingulodinium polyedrum* to laminar and turbulent flow. *Limnology and Oceanography* 44, 1423–1435.
- Lazier, J.R.N., Mann, K.H., 1989. Turbulence and the diffusive layers around small organisms. *Deep-Sea Research Part A* 36, 1721–1733.
- Lewis, N.I., Xu, W., Jericho, S.K., Kreuzer, H.J., Jericho, M.H., Cembella, A.D., 2006. Swimming speed of three species of *Alexandrium* (Dinophyceae) as determined by digital in-line holography. *Phycologia* 45, 61–70.
- Lien, R.-C., Sanford, T.B., 2004. Turbulence spectra and local similarity scaling in a strongly stratified oceanic bottom boundary layer. *Continental Shelf Research* 24, 375–392.
- Lu, Y., Lueck, R.G., Huang, D., 2000. Turbulence characteristics in a tidal channel. *Journal of Physical Oceanography* 30, 855–867.
- Lueck, R., Huang, D., 1999. Dissipation measurement with a moored instrument in a swift tidal channel. *Journal of Atmospheric and Oceanic Technology* 16, 1499–1505.
- Lueck, R.G., Huang, D., Newman, D., Box, J., 1997. Turbulence measurement with a moored instrument. *Journal of Atmospheric and Oceanic Technology* 14, 143–161.
- MacKenzie, B.R., Leggett, W.C., 1993. Wind-based models for estimating the dissipation rates of turbulent energy in aquatic environments: empirical comparisons. *Marine Ecological: Progress Series* 94, 207–216.
- Mackie, G.O., Singla, C.L., Thiriot-Quievreux, C., 1976. Nervous control of ciliary activity in gastropod larvae. *Biological Bulletin* 151, 182–199.
- MacKinnon, J.A., Gregg, M.C., 2003. Shear and baroclinic energy flux on the summer New England shelf. *Journal of Physical Oceanography* 33, 1462–1475.
- MacKinnon, J.A., Gregg, M.C., 2005a. Near-inertial waves on the New England shelf: the role of evolving stratification, turbulent dissipation, and bottom drag. *Journal of Physical Oceanography* 35, 2408–2424.
- MacKinnon, J.A., Gregg, M.C., 2005b. Spring mixing: turbulence and internal waves during restratification on the New England shelf. *Journal of Physical Oceanography* 35, 2425–2443.
- Martens, E.A., Wadhwa, N., Jacobsen, N.S., Lindemann, C., Andersen, K.H., Visser, A., 2015. Size structures sensory hierarchy in ocean life. *Proceedings of the Royal Society B* 282, 20151346.
- Massel, S.R., 1996. *Ocean Surface Waves: Their Physics and Prediction*. World Scientific.
- Maxey, M.R., Riley, J.J., 1983. Equation of motion for a small rigid sphere in a nonuniform flow. *Physics of Fluids* 26, 883–889.
- McDonald, K.A., 2012. Earliest ciliary swimming effects vertical transport of planktonic embryos in turbulence and shear flow. *Journal of Experimental Biology* 215, 141–151.
- McManus, M.A., Cheriton, O.M., Drake, P.J., Holliday, D.V., Storlazzi, C.D., Donaghay, P.L., Greenlaw, C.F., 2005. Effects of physical processes on structure and transport of thin zooplankton layers in the coastal ocean. *Marine Ecological: Progress Series* 301, 199–215.
- Mei, C.C., 1989. *The Applied Dynamics of Ocean Surface Waves*. World Scientific Publishing Co., Singapore.
- Mei, R., 1996. Velocity fidelity of flow tracer particles. *Experiments in Fluids* 22, 1–13.
- Menden-Deuer, S., Grünbaum, D., 2006. Individual foraging behaviors and population distributions of a planktonic predator aggregating to phytoplankton thin layers. *Limnology and Oceanography* 51, 109–116.
- Mogami, Y., Ishii, J., Baba, S.A., 2001. Theoretical and experimental dissection of gravity-dependent mechanical orientation in gravitactic microorganisms. *Biological Bulletin* 201, 26–33.
- Monahan, A.H., 2006. The probability distribution of sea surface wind speeds. Part 1: Theory and SeaWinds observations. *Journal of Climate* 19, 497–520.
- Mooney, T.A., Hanlon, R.T., Christensen-Dalsgaard, J., Madsen, P.T., Ketten, D.R., Nachtigall, P.E., 2010. Sound detection by the longfin squid (*Loligo pealeii*) studied with auditory evoked potentials: sensitivity to low-frequency particle motion and not pressure. *Journal of Experimental Biology* 213, 3748–3759.
- Moum, J.N., Farmer, D.M., Smyth, W.D., Armi, L., Vagle, S., 2003. Structure and generation of turbulence at interfaces strained by internal solitary waves propagating shoreward over the continental shelf. *Journal of Physical Oceanography* 33, 2093–2112.
- Moum, J.N., Gregg, M.C., Lien, R.C., Carr, M.E., 1995. Comparison of turbulence kinetic energy dissipation rate estimates for two ocean microstructure profilers. *Journal of Atmospheric and Oceanic Technology* 12, 346–366.
- Moum, J.N., Lien, R.-C., Perlin, A., Nash, J.D., Gregg, M.C., Wiles, P.J., 2009. Sea surface cooling at the equator by subsurface mixing in tropical instability waves. *Nature Geoscience* 2, 761–765.
- Moum, J.N., Osborn, T.R., Crawford, W.R., 1986. Pacific equatorial turbulence: revisited. *Journal of Physical Oceanography* 16, 1516–1522.
- Mouri, H., Takaoka, M., Hori, A., Kawashima, Y., 2002. Probability density function of turbulent velocity fluctuations. *Physical Review E* 65, 056304:1–056304:7.

- Naitoh, Y., Eckert, R., 1969. Ionic mechanisms controlling behavioral responses of paramecium to mechanical stimulation. *Science* 164, 963–965.
- Oakey, N.S., 1982. Determination of the rate of dissipation of turbulent energy from simultaneous temperature and velocity shear microstructure measurements. *Journal of Physical Oceanography* 12, 256–271.
- Oakey, N.S., Elliott, J.A., 1982. Dissipation within the surface mixed layer. *Journal of Physical Oceanography* 12, 171–185.
- Osborn, T., Farmer, D.M., Vagle, S., Thorpe, S.A., Cure, M., 1992. Measurements of bubble plumes and turbulence from a submarine. *Atmosphere-Ocean* 30, 419–440.
- Osborn, T.R., Bilodeau, L.E., 1980. Temperature microstructure in the equatorial Atlantic. *Journal of Physical Oceanography* 10, 66–82.
- Paffenhöfer, G.-A., 1998. On the relation of structure, perception and activity in marine planktonic copepods. *Journal of Marine Systems* 15, 457–473.
- Pepper, R.E., Jaffe, J.S., Variano, E., Koehl, M.A.R., 2015. Zooplankton in flowing water near benthic communities encounter rapidly fluctuating velocity gradients and accelerations. *Marine Biology* 162, 1939–1954.
- Peters, H., 1997. Observations of stratified turbulent mixing in an estuary: neap-to-spring variations during high river flow. *Estuarine, Coastal and Shelf Science* 45, 69–88.
- Peters, H., Bokhorst, R., 2000. Microstructure observations of turbulent mixing in a partially mixed estuary. Part I: Dissipation rate. *Journal of Physical Oceanography* 30, 1232–1244.
- Peterson, E.W., Hennessey Jr., J.P., 1978. On the use of power laws for estimates of wind power potential. *Journal of Applied Meteorology* 17, 390–394.
- Phillips, O.M., 1966. *The Dynamics of the Upper Ocean*. Cambridge University Press.
- Pierson Jr., W.J., Moskowitz, L., 1964. A proposed spectral form for fully developed wind seas based on the similarity theory of S.A. Kitaigorodskii. *Journal of Geophysical Research* 69, 5181–5190.
- Rakow, K.C., Graham, W.M., 2006. Orientation and swimming mechanics by the scyphomedusa *Aurelia* sp. in shear flow. *Limnology and Oceanography* 51, 1097–1106.
- Reidenbach, M.A., Koseff, J.R., Koehl, M.A.R., 2009. Hydrodynamic forces on larvae affect their settlement on coral reefs in turbulent, wave-driven flow. *Limnology and Oceanography* 54, 318–330.
- Rippeth, T.P., Simpson, J.H., Williams, E., Inall, M.E., 2003. Measurement of the rates of production and dissipation of turbulent kinetic energy in an energetic tidal flow: Red Wharf Bay revisited. *Journal of Physical Oceanography* 33, 1889–1901.
- Roberts, W., Le Hir, P., Whitehouse, R.J.S., 2000. Investigation using simple mathematical models of the effect of tidal currents and waves on the profile shape of intertidal mudflats. *Continental Shelf Research* 20, 1079–1097.
- Rosman, J.H., Hench, J.L., Koseff, J.R., Monismith, S.G., 2008. Extracting Reynolds stresses from acoustic Doppler current profiler measurements in wave-dominated environments. *Journal of Atmospheric and Oceanic Technology* 25, 286–306.
- Rothschild, B.J., Osborn, T.R., 1988. Small-scale turbulence and plankton contact rates. *Journal of Plankton Research* 10, 465–474.
- Rousseau, S., Kunze, E., Dewey, R., Bartlett, K., Dower, J., 2010. On turbulence production by swimming marine organisms in the open ocean and coastal waters. *Journal of Physical Oceanography* 40, 2107–2121.
- Rubinow, S.I., Keller, J.B., 1961. The transverse force on a spinning sphere moving in a viscous fluid. *Journal of Fluid Mechanics* 11, 447–459.
- Saffman, P.G., 1965. The lift on a small sphere in slow shear flow. *Journal of Fluid Mechanics* 22, 385–400.
- Saiz, E., Kiørboe, T., 1995. Predatory and suspension feeding of the copepod *Acartia tonsa* in turbulent environments. *Marine Ecological: Progress Series* 122, 147–158.
- Sandstrom, H., Oakey, N.S., 1995. Dissipation in internal tides and solitary waves. *Journal of Physical Oceanography* 25, 604–614.
- Sanford, T.B., Lien, R.-C., 1999. Turbulent properties in a homogeneous tidal bottom boundary layer. *Journal of Geophysical Research* 104, 1245–1257.
- Scully, M.E., Geyer, W.R., Trowbridge, J.H., 2011. The influence of stratification and nonlocal turbulent production on estuarine turbulence: an assessment of turbulence closure with field observations. *Journal of Physical Oceanography* 41, 166–185.
- Shaw, W.J., Trowbridge, J.H., Williams III, A.J., 2001. Budgets of turbulent kinetic energy and scalar variance in the continental shelf bottom boundary layer. *Journal of Geophysical Research* 106, 9551–9564.
- Sherman, D.J., Nordstrom, K.F., Jackson, N.L., Allen, J.R., 1994. Sediment mixing-depths on a low-energy reflective beach. *Journal of Coastal Research* 10, 297–305.
- Simpson, J.H., Brown, J., Matthews, J., Allen, G., 1990. Tidal straining, density currents, and stirring in the control of estuarine stratification. *Estuaries* 13, 125–132.
- Simpson, J.H., Crawford, W.R., Rippeth, T.P., Campbell, A.R., Cheok, J.V.S., 1996. The vertical structure of turbulent dissipation in shelf seas. *Journal of Physical Oceanography* 26, 1579–1590.
- Singarajah, K.V., 1975. Escape reactions of zooplankton: effects of light and turbulence. *Journal of the Marine Biological Association UK* 55, 627–639.
- Sleigh, M.A., Blake, J.R., 1977. Methods of ciliary propulsion and their size limitations. In: Pedley, T. (Ed.), *Scale Effects in Animal Locomotion*. Academic Press, pp. 243–256.
- Smith, S.D., 1980. Wind stress and heat flux over the ocean in gale force winds. *Journal of Physical Oceanography* 10, 709–726.
- Soloviev, A., Lukas, R., 2003. Observation of wave-enhanced turbulence in the near-surface layer of the ocean during TOGA COARE. *Deep Sea Research, Part I* 50, 371–395.
- Stacey, M.T., Monismith, S.G., Burau, J.R., 1999. Measurements of Reynolds stress profiles in unstratified tidal flow. *Journal of Geophysical Research* 104, 10,933–10,949.
- Stacey, M.T., Ralston, D.K., 2005. The scaling and structure of the estuarine bottom boundary layer. *Journal of Physical Oceanography* 35, 55–71.
- Stake, J.L., Sammarco, P.W., 2003. Effects of pressure on swimming behavior in planula larvae of the coral *Porites astreoides* (Cnidaria, Scleractinia). *Journal of Experimental Marine Biology and Ecology* 288, 181–201.
- Stevens, A.W., Lacy, J.R., 2012. The influence of wave energy and sediment transport on seagrass distribution. *Estuaries and Coasts* 35, 92–108.
- Stewart, W.J., Cardenas, G.S., McHenry, M.J., 2013. Zebrafish larvae evade predators by sensing water flow. *Journal of Experimental Biology* 216, 388–398.
- Styles, R., Glenn, S.M., 2005. Long-term sediment mobilization at a sandy inner shelf site, LEO-15. *Journal of Geophysical Research* 110, C04S90.
- Taylor, G.I., 1935. Statistical theory of turbulence. *Proceedings of the Royal Society of London, Series A: Mathematical and Physical Sciences* 151, 421–444.
- Tennekes, H., Lumley, J.L., 1972. *A First Course in Turbulence*. MIT Press, Cambridge, MA.
- Terray, E.A., Donelan, M.A., Agrawal, Y.C., Drennan, W.M., Kahma, K.K., Williams III, A.J., Hwang, P.A., Kitaigorodskii, S.A., 1996. Estimates of kinetic energy dissipation under breaking waves. *Journal of Physical Oceanography* 26, 792–807.
- Tesson, B., Latz, M.L., 2015. Mechanosensitivity of a rapid bioluminescence reporter system assessed by atomic force microscopy. *Biophysical Journal* 108, 1341–1351.
- Thomson, J., Polagye, B., Durgesh, V., Richmond, M.C., 2012. Measurements of turbulence at two tidal energy sites in Puget Sound, WA. *IEEE Journal of Oceanic Engineering* 37, 363–374.
- Thorpe, S.A., Osborn, T.R., Jackson, J.F.E., Hall, A.J., Lueck, R.G., 2003. Measurements of turbulence in the upper-ocean mixing layer using Autosub. *Journal of Physical Oceanography* 33, 122–145.
- Tiselius, P., Jonsson, P.R., 1990. Foraging behaviour of six calanoid copepods: observations and hydrodynamic analysis. *Marine Ecological: Progress Series* 66, 23–33.
- Titelman, J., 2001. Swimming and escape behavior of copepod nauplii: implications for predator-prey interactions among copepods. *Marine Ecological: Progress Series* 213, 203–213.
- Traykovski, P., 2007. Observations of wave orbital scale ripples and a nonequilibrium time-dependent model. *Journal of Geophysical Research* 112, C06026.
- Trowbridge, J., Elgar, S., 2001. Turbulence measurements in the surf zone. *Journal of Physical Oceanography* 31, 2403–2417.
- Trowbridge, J., Madsen, O.S., 1984. Turbulent wave boundary layers: 1. Model formulation and first-order solution. *Journal of Geophysical Research* 89, 7989–7997.
- Trowbridge, J.H., 1998. On a technique for measurement of turbulent shear stress in the presence of surface waves. *Journal of Atmospheric and Oceanic Technology* 15, 290–298.
- Trowbridge, J.H., Geyer, W.R., Bowen, M.M., Williams III, A.J., 1999. Near-bottom turbulence measurements in a partially mixed estuary: turbulent energy balance, velocity structure, and along-channel momentum balance. *Journal of Physical Oceanography* 29, 3056–3072.
- Van Atta, C.W., Antonia, R.A., 1980. Reynolds number dependence of skewness and flatness factors of turbulent velocity derivatives. *Physics of Fluids* 23, 252–257.
- Visser, A.W., 2001. Hydromechanical signals in the plankton. *Marine Ecological: Progress Series* 222, 1–24.
- Visser, A.W., Mariani, P., Pigolotti, S., 2009. Swimming in turbulence: zooplankton fitness in terms of foraging efficiency and predation risk. *Journal of Plankton Research* 31, 121–133.
- Vogel, S., 1994. *Life in Moving Fluids*, 2nd edition. Princeton University Press, Princeton, NJ.
- Voth, G.A., La Porta, A., Crawford, A.M., Alexander, J., Bodenschatz, E., 2002. Measurement of particle accelerations in fully developed turbulence. *Journal of Fluid Mechanics* 469, 121–160.
- Webster, D.R., Young, D.L., Yen, J., 2015. Copepods' response to Burgers' vortex: deconstructing interactions of copepods with turbulence. *Integrative and Comparative Biology* 55, 706–718.
- Welch, J.M., Forward Jr., R.B., 2001. Flood tide transport of blue crab, *Callinectes sapidus*, postlarvae: behavioral responses to salinity and turbulence. *Marine Biology* 139, 911–918.
- Wendt, D.E., 2000. Energetics of larval swimming and metamorphosis in four species of Bugula (Bryozoa). *Biological Bulletin* 198, 346–356.
- Whalen, C.B., Talley, L.D., MacKinnon, J.A., 2012. Spatial and temporal variability of global ocean mixing inferred from Argo profiles. *Geophysical Research Letters* 39, L18612.
- Woodson, C.B., Webster, D.R., Weissberg, M.J., Yen, J., 2007. The prevalence and implications of copepod behavioral responses to oceanographic gradients and biological patchiness. *Integrative and Comparative Biology* 47, 831–846.
- Woodson, C.B., Webster, D.R., Weissberg, M.J., Yen, J., 2005. Response of copepods to physical gradients associated with structure in the ocean. *Limnology and Oceanography* 50, 1552–1564.
- Yamazaki, H., Lueck, R., 1990. Why oceanic dissipation rates are not lognormal. *Journal of Physical Oceanography* 20, 1907–1918.
- Yen, J., 1988. Directionality and swimming speeds in predator-prey and male-female interactions of *Euchaeta rimana*, a subtropical marine copepod. *Bulletin of Marine Science* 43, 395–403.
- Yen, J., Lenz, P.H., Gassie, D.V., Hartline, D.K., 1992. Mechanoreception in marine copepods: electrophysiological studies on the first antennae. *Journal of Plankton Research* 14, 495–512.
- Young, C.M., 1995. Behavior and locomotion during the dispersal phase of larval life. In: McEdward, L. (Ed.), *Ecology of Marine Invertebrate Larvae*. CRC Press, pp. 249–278.